Mapping of a buried basement combining aeromagnetic, gravity and petrophysical data: The substratum of southwest Paris Basin, France

Julien Baptiste, Guillaume Martelet, Michel Faure, Laurent Beccaletto, Pierre-Alexandre Reninger, José Perrin, Yan Chen

Mapping of a buried basement combining aeromagnetic, gravity and petrophysical data: the substratum of southwest Paris Basin, France

*Julien Baptiste[1,2], Guillaume Martelet[2], Michel Faure[1], Laurent Beccaletto[2], Pierre-Alexandre Reninger[2], José Perrin[2], Yan Chen[1],

[1] Institut des Sciences de la Terre d'Orléans, UMR 7327, Université d'Orléans, Campus Géosciences, 1A rue de la Férollerie, 45071 Orléans Cedex 2

[2] Bureau de Recherche Géologique et Minière (BRGM), UMR 7327, 3 avenue Claude Guillemin, BP 36009, 45060 Orléans Cedex 2.

* Corresponding author: j.baptiste@brgm.fr

Abstract

Aeromagnetic and gravity data have proven to be among the most effective methods for mapping deeply buried basin/basement interfaces. However, the data interpretation generally suffers from ambiguities, due to the non-uniqueness of the gravity and magnetic signatures. Here, we tie the gravity and magnetic signatures with a petrophysical characterization of the lithologies outcropping around the French Paris Basin. Our methodology investigates the lithology and structure of its hidden Variscan substratum at the junction between the Armorican Massif and Massif Central. Our approach is based on the combination of potential field data, magnetic susceptibilities measured in the field, density values of sample rocks and information documented in boreholes, in order to propose a new interpretative geological map of the buried substratum of the Paris Basin. The petrophysical description is combined with geophysical patterns of the substratum, mapped through statistical unsupervised classification of suitably selected magnetic and gravity maps. The first step of interpretation consists in extending the outcropping major structures below the Meso-Cenozoic sedimentary cover of the Paris Basin. The litho-structural units, in between these major structures, are then interpreted separately. The second step consists in assigning lithologies within each unit, with respect to its magnetization and density (as derived from the petrophysical compilation), and mapping its extension under cover, integrating punctual borehole information. Overall, with a special emphasis on relating geophysical signatures and petrophysical characteristics of litho-structural units, this methodology permits a precise structural and lithological cartography of a segment of the buried Variscan substratum. In the southwestern part of the Paris Basin, this approach reveals: i) the limited eastward extension of Central Brittany, ii) the eastward extension of the major Cholet fault, iii) the emphasis on N150E-N160E striking fault and

39 their N30E conjugates, controlling the opening of Permo-Carboniferous basins, and iv) the
40 eastward extension of the Eo-Variscan suture.

41 **Keywords:** aeromagnetic, gravity, Paris Basin, Variscan substratum, petrophysical data,
42 undercover mapping

43 1. Introduction

44 The European Variscan belt belongs to a several thousand-km-long Late Paleozoic orogen
45 extending from the Appalachians in the eastern North America, to Polish Sudetes, through
46 the Mauritanides in West Africa. This belt, formed by Proterozoic to Carboniferous rocks,
47 constitutes the Pre-Mesozoic basement of a large part of Western and Central Europe. In
48 France, the Variscan belt presently crops out in several massifs, namely: Massif Central,
49 Armorican, Ardennes, and Vosges Massifs and in the basement of the Cenozoic Alpine and
50 Pyrenean belts. The continuity between these massifs is hidden by several Mesozoic to
51 Cenozoic sedimentary basins, such as the Paris or Aquitaine Basin (Fig. 1)
52 The Paris Basin is an intraplate sedimentary basin, set up on the Variscan substratum that
53 crops out in the above massifs (Pomerol, 1978; Mégnien; 1980, Perrodon and Zabek, 1990;
54 Guillocheau et *al.*, 2000; Chantraine et *al.*, 2003) (Fig. 1). It is well known that lithologies
55 and structures of the southern part of the Armorican Massif and the Massif Central are
56 closely related (Autran and Lameyre, 1980; Matte and Hirn, 1988; Virlogeux et *al.*, 1999;
57 Faure et *al.*, 2005; Cartannaz et *al.*, 2006; Gébelin et *al.*, 2007; Ballèvre et *al.*, 2009; Rolin
58 et *al.*, 2009); however, their connection is still poorly known, as it hidden by the Meso-
59 Cenozoic Paris Basin sedimentary cover. Both massifs are composed of several litho-
60 tectonic units separated by crustal-scale shear zones, such as the North Armorican Shear
61 Zone (NASZ) and the South Armorican Shear Zone (SASZ), in the Armorican Massif or the
62 Marche Fault in the Massif Central (Fig. 1). In addition, the Nort-sur-Erdre fault of the

63 Armorican Massif (NSE F.; Fig. 1) is acknowledged as the Eo-Variscan suture (Fig. 1)
64 (Matte, 1986; Le Corre et *al.*, 1991; Ballèvre et *al.*, 1992; Lardeux and Cavet, 1994; Faure
65 et *al.*, 1997; Cartier et *al.*, 2001; Bitri et *al.*, 2003). The eastward extension of the Armorican
66 litho-structural units has already been integrated in large-scale geodynamic reconstructions
67 of the Variscan belt, either based on geological evidence (e.g. Matte, 1986; Faure et *al.*,
68 2005; Ballèvre et *al.*, 2009; Martínez-Catalán, 2012, Edel *et al.*, 2015) or on low to medium-
69 resolution regional geophysics (e.g. Edel, 2008). There is no agreement on the limits and
70 nature of the units, and geodynamic significance is still under debate. A way to ascertain
71 these models would be to fill the geological observation gap caused by the Meso-Cenozoic
72 sedimentary cover of the Paris Basin by new high resolution data.
73 In the second half of the 20th century, the Paris Basin substratum started being investigated
74 using gravity data (Goguel and Francia, 1954), deep boreholes (Lienhardt, 1961) or deep
75 seismic profiles (Matte and Hirn, 1988). A combination of gravity and intermediate to low
76 resolution aeromagnetic data was used in the southwestern part of the Paris Basin
77 (Weber, 1973). The extension of this last study to the entire Paris Basin led to the first
78 version of a pseudo-lithological and structural sketch of the pre-Mesozoic substratum of the
79 Paris Basin (Debeglia and Weber, 1980). More recently, on the basis of the combination of
80 new high resolution magnetic data and updated gravity data, Martelet et *al.*, (2013)
81 proposed a method to characterize the substratum geometry of the central-south part of the
82 Paris Basin, but no detailed lithological interpreted map was produced yet.
83 In addition, a map of the buried substratum around the Poitou High was proposed on the
84 base of detailed structural analysis and drilling information (Rolin and Colchen, 2001).
85 Because we now benefit from recent high resolution aeromagnetic data on the entire
86 southwestern part of the Paris Basin, we are now able to address the litho-structural pattern
87 of its buried substratum with an unprecedented resolution. Complemented by a

characterization of the field petrophysical properties of the various litho-structural units, our work ascertain cartographic interpretations of the geophysical signatures. Our methodology emphasizes the processing of interpretation of potential field data to derive a high-resolution structural map. Combining the latter with field petrophysical properties, lithologies were then interpreted in each litho-structural unit, leading to a new geological map of the Paris Basin substratum.

The extensions of the litho-structural units as well as the lithologies of the Variscan and their regional geological implications are further discussed.

2. Geological setting

The Paris Basin is a low subsidence Meso-Cenozoic sedimentary basin. It is composed of silico-clastic and calcareous rocks (Pomerol, 1978; Mégnien, 1980; Perrodon and Zabek, 1990; Guillocheau et *al.*, 2000; Beccaletto et *al.*, 2011). It is set up on a Variscan substratum including Permo-Carboniferous basins. In the study area, the formations constituting the Variscan substratum of the Paris Basin laterally outcrop in the Armorican Massif to the west and the Massif Central, to the south, respectively (Fig. 2a).

The Armorican Massif is composed of several litho-structural units separated by crustal-scale faults and characterized by distinct lithologies and tectonic evolutions (Fig. 2a). The North Armorican Shear Zone (NASZ; Chauris, 1969; Watts and Williams, 1979), the northern and the southern branches of the South Armorican Shear Zone (NBSASZ and SBSASZ, respectively) (Jégouzo, 1980) and the Nort-sur-Erdre fault (NSE) are the main Variscan structures of the central and southeastern part of the Armorican Massif (Fig. 2a). The NASZ and the SBSASZ delimit the Central Brittany to the north and south, respectively (Fig. 2a). Central Brittany consists of folded and weakly metamorphosed Neoproterozoic

112 sediments, unconformably overlain by weakly deformed Paleozoic sediments, intruded by
113 Carboniferous granites (Fig. 2b) (Vernhet et *al.*, 2009). Located along the NASZ, the
114 southerly early Carboniferous Laval basin is superimposed on the Neoproterozoic to
115 Paleozoic series (Fig. 2b). It is composed of early Carboniferous sedimentary rocks
116 interbedded with acidic and basic volcanic rocks (Le Hérissé and Plaine, 1982). The Laval
117 basin was folded during the Late Carboniferous (Houlgatte *et al.*, 1988).
118 Between the NBSASZ and the NSE fault, the Paleozoic series of the St-Georges-sur-Loire
119 unit overthrusts to the NW the Lanvaux unit (Fig. 2a). The NW-SE striking Lanvaux unit is
120 composed of Neoproterozoic and early Cambrian metasediments overlain by Paleozoic
121 weakly metamorphosed sediments (Lardeux and Cavet, 1994), and intruded by an early
122 Ordovician granite deformed into an orthogneiss (Fig. 2b), called the St-Clément-de-la-
123 Place (Vidal, 1980). This orthogneiss is intruded by two granitic plutons: i) the Bécon
124 granite (Chauris and Lucas, 1964; Cavet et *al.*, 1970, 1976) and ii) the St-Lambert
125 granodiorite showing S/C structures, emplaced during to the Carboniferous dextral shearing
126 of the NBSASZ (Faure and Cartier, 1998). The Lanvaux unit experienced a polyphase
127 deformation (Faure and Cartier, 1998). The foliation attitude documents an antiform, the
128 core of which is constituted by the orthogneiss. Outcropping at the junction between the
129 Lanvaux and St-Georges-sur Loire unit, the Questembert leucogranite, emplaced during the
130 late Carboniferous (Tartèse et *al.*, 2011a, 2011b) is a syn-tectonic granite related to the
131 SASZ shearing (Berthé et *al.*, 1979; Bernard-Griffiths et *al.*, 1985).
132 To the south, the St-George-sur-Loire unit is divided into two sub-units (Fig. 2a): the blocky
133 sub-unit in the south overthrusts to the NW the northerly Sandstone-Pelite sub-unit (Cartier
134 et *al.*, 2001; Cartier and Faure, 2004).
135 The south of Nort-sur-Erdre fault is a metamorphic nappe stack: described in the southern
136 part of the Armorican Massif (Burg, 1981; Matte, 1991; Bosse et *al.*, 2000; Le Hébel et *al.*,

137 2002) and in the northern part of the Massif Central (Quenardel and Rolin, 1984; Faure et
138 *al.*, 1990). The structure and the lithology of the metamorphic Champtoceaux Complex in
139 the Armorican Massif and of the Aigurande Plateau in the Massif Central are quite similar
140 (Fig. 2b) (e.g. Faure et *al.*, 2005; Ballèvre et *al.*, 2009). However the Armorican Massif
141 exposes peculiar units absent in the Massif Centr*al.* The uppermost unit of the nappe stack,
142 called the Mauges nappe (Fig. 2a), consists of Neoproterozoic metagrauwackes
143 interbedded with meta-volcanics (Wyns and Le Métour, 1983; Cabanis and Wyns, 1986;
144 Wyns et *al.*, 1998), and unconformably overlain by Cambrian sedimentary rocks and felsic
145 volcanites, and Ordovician sandstones (Fig. 2b). This Paleozoic sedimentary and volcanic
146 series is widely exposed in the Choletais area (Cavet et *al.*, 1966). The Cambrian Thouars
147 microgranitic massif associated with basic rocks (gabbros, quartz diorites) intrudes within
148 the Neoproterozoic micaschists, the volcanic series and the dyke complex (Fig. 2b;
149 Thiéblemont et *al.*, 1987, 2001). To the north of the Mauges nappe, the Ancenis basin is
150 located along the NSE fault (Fig. 2a). It is made of Devonian to early Carboniferous
151 deposits (Fig. 2b) (Cavet et *al.*, 1971; Ballèvre and Lardeux., 2005), superimposing the
152 Neoproterozoic micaschists (Fig. 2b).
153 Another unit, exposed uniquely in the Armorican Massif is the "Drain Unit" consisting of
154 serpentinite, gabbro, basalt and siliceous sedimentary rocks, interpreted as dismembered
155 ophiolites along the Eo-variscan suture (Marchand, 1981; Ballèvre et *al.*, 1994; Faure et *al.*,
156 2008). The underlying unit, called the Champtoceaux complex, is an imbrication of crustal-
157 scale thrust sheets characterized by highly deformed and metamorphosed gneiss and
158 eclogites (Marchand, 1981; Ballèvre et *al.*, 1989, 1994; Bosse et *al.*, 2000). Lastly, the
159 lowermost unit exposed in this area consists of a micaschist and paragneiss suite, named
160 the Mauves-sur-Loire series (Fig. 2b). The entire stack of nappes from the Mauges nappe
161 to the Mauves-sur-Loire series is folded in a km-scale antiform with a steeply eastward

plunging axis probably related to the dextral shearing of the SASZ (Martelet et *al.*, 2004). Carboniferous plutons occupy the core of this antiform (e.g. Wyns et *al.*, 1998).

The Aigurande Plateau also consists of a stack of metamorphic nappes, refolded as an ENE-SSW striking antiform, and intruded by several two-mica granitic plutons (Quenardel and Rolin, 1984; Faure et *al.*, 1990). From top to bottom, the litho-tectonic units are characterized by: i) the Upper Gneiss Unit (UGU) composed of a bimodal magmatic series, named leptynite-amphibolite complex with eclogites, and migmatites; ii) the Lower Gneiss Unit (LGU) made of metagrauwackes, micaschists, metarhyolites and amphibolites that never experienced a HP metamorphism; iii) the Para-autochthonous Unit composed of low-grade micaschists (Fig. 2b). The left-lateral Marche fault, main Variscan structure of the northern part of the Massif Central (e.g. Quenardel and Rolin, 1984), is the southern boundary of the Aigurande Plateau (Fig. 2a). A reasonable correlation between the Champtoceaux Complex and the Mauves-sur-Loire Unit in the Armorican Massif and the UGU and LGU in the Massif Central, respectively has been proposed (e.g. Faure et *al.*, 2005).

Previous structural and lithological analyses within the Poitou High (Rolin and Colchen, 2001) documented the close connection between the Haut Bocage unit and the Confolentais area. In the Poitou High, the substratum that crops out in rare valleys is made of Carboniferous granite. Below the sedimentary cover of the Poitou High, the SBSASZ eastward extension splits into several branches which separate structures and lithologies of the Haut Bocage and Confolentais units (Fig. 2a) (Rolin and Colchen, 2001). The Haut Bocage unit is composed of anatectic gneiss and Neoproterozoic micaschists (Fig. 2b). The Confolentais unit is made of granites, metavolcanites and metasediments belonging to the UGU (Fig. 2b). Both units are intruded by late Devonian gabbro, granodiorites and diorites that also crop out along the left-lateral Marche fault (Peiffer, 1986; Cuney et *al.*, 1993; Pin

187 and Paquette, 2002). In the Confolentais area can be found the westernmost expression of
188 the Limousin tonalite belt (Bernard-Griffiths et *al.*, 1985; Peiffer, 1986).
189

190 ## 3. Aeromagnetic and gravity data

191 ### *3.1. Processing of aeromagnetic data*

192 Magnetic measurements monitor the spatial variations of magnetic properties of the
193 underground, from the surface of the Earth down to several kilometers. The French
194 Geological Survey (BRGM) conducted a fixed-wing magnetic survey in 1998 over Brittany
195 (Bonijoly et *al.*, 1999; Truffert et *al.*, 2001) and from August 2008 to October 2010 over the
196 Pays de la Loire (PaL) and Région Centre (Martelet et *al.*, 2013) covering the Armorican
197 Massif and the southwestern part of the Paris Basin (Fig. 3a). These surveys were flown at
198 an average 85 m and 120 m ground clearance for Région Centre, PaL and Brittany,
199 respectively. For the three surveys, the flight path was oriented N-S, with a line-spacing of
200 500 m reduced to 250 m over key areas for the Brittany survey and 1 km reduced to 500 m
201 for PaL and Région Centre surveys; perpendicular control tie lines were also flown every
202 10 km. The surveys overlap with each other on a 3 to 5 km band at their periphery. In order
203 to get rid of punctual artifacts related to human activities, the data were upward continued
204 to an elevation of 600 m. This removed the short wavelength cultural noise without
205 significantly smoothing the data, with regards to the aims and regional extent of the study.
206 Magnetic anomaly 250 m regular grids were produced using the minimum curvature
207 gridding method (Taylor and Mason, 1972), separately, for each survey.
208 In addition three grid transforms were applied to emphasize various properties of the buried
209 substratum:

210 - The reduction to the pole (RTP; Fig. 3b): it contributes to simplify the magnetic signal
211 interpretation (Blakely, 1996). Taking into account the Earth field direction, this

operator relocates the magnetic anomaly on top of its causative body. When induced magnetization predominates, anomaly bipolarities are removed, so that RTP positive anomalies indicate a local increase of magnetic susceptibility at depth.

- The vertical derivative (Fig. 3c): it enhances local signal gradients while regional trends are removed. Magnetization in the Meso-Cenozoic Paris Basin is weak and sedimentary cover thickness vary smoothly over large distances; therefore, they generate long wavelength components in the magnetic map, which are removed by the vertical gradient operator. Consequently the map of the magnetic vertical gradient highlights the magnetic contrasts within the underlying substratum (e.g. Weber, 1973; .Martelet et *al.*, 2013).
- The Tilt derivative (TILT) or Tilt angle processing (e.g. Miller and Singh, 1994; Verduzco et *al.*, 2004) is powerful for structural interpretation as it depicts equally the edge of deep and shallow magnetic sources (Miller and Singh, 1994). It is an effective method for mapping contacts or faults, weakly contrasted magnetized bodies, located under a sedimentary cover (Fairhead et *al*., 2011). The TILT map was used to highlight the structures of the underlying substratum and the magnetic body contours which are defined by the zero value in the TILT map (Fig. 3d).

The vertical derivative and the tilt derivative operators were applied on the anomaly reduced to the pole (RTP). In order to avoid artifacts at survey junctions, the magnetic transforms were applied separately, survey by survey, before merging. The merge of the three magnetic surveys was carefully achieved, using a standard grid stitching algorithm.

3.2. Processing of gravity data

Gravity data derive from the compilation of ground gravity surveys conducted in France since the middle of the 20th century and compiled in the Banque Gravimétrique de la France (BGF) (Martelet, et *al.*, 2009). In the study area, the average station coverage is about 1 station/km². Data are tied to the CGF65 base station network. In order to derive the Bouguer anomaly, all standard corrections are included, with a reference density of 2600 kg/m3, and terrain corrections computed to a distance of 167 km (Martelet et *al.*, 2002). Taking into account the accuracy of 1) the network, 2) the gravity measurements and their positioning and 3) the terrain corrections, the RMS error on the Bouguer anomaly is 0.32 mGal in the study area. The Bouguer anomaly map presented in Fig. 4a locates the main regional density contrasts, from the surface down to several kilometers at depth.

A map of the vertical derivative of the Bouguer anomaly is presented in Fig. 4b. The first order of the vertical gradient of the Bouguer anomaly has long been used for separating close structures (Elkins, 1951; Gérard and Griveau, 1972; Goguel, 1972). Here, this operator is used to highlight density contrasts within the Paris Basin substratum. As for the magnetic map, the regional effect of the Meso-Cenozoic sedimentary pile results in smooth and long wavelength signals and is therefore strongly attenuated by this operator (see Martelet et *al.*, 2013 for more details). Positive and negative signals of the vertical gradient feature relatively high and low density rocks at depth, respectively.

4. Measurements of field rock properties

Gravity and magnetic map usually display “averaged” geophysical signatures of geological bodies as compared to the lithological variations at the outcrop scale; the discrimination of the magnetic and gravity causative lithologies suffering from ambiguities. An extensive campaign of petrophysical sampling and measurements was conducted in order to take into

account this scale effect in our geophysical maps interpretation. It was designed to derive reliable petrophysical “statistic signatures” for the main lithologies encountered in the study area.

4.1 Magnetic susceptibility

The magnetic susceptibility of a rock refers to its ability to become magnetized by an external magnetic field such as the Earth’s field (e.g. Dearing, 1999). Rocks have various magnetic responses due to their magnetic properties, which to the first order, depend on the volume content of magnetite (Clark and Emerson, 1991). Magnetic susceptibility field measurements were carried out using a hand-held kappameter (KT-9, Exploranium, Canada). The measuring range of KT-9 susceptibility meters is from -999 to 999 x 10–3 SI units with a sensitivity of 1 x 10-5 SI. Because reproducibility of measures is influenced by the irregularity of the rock surface (Lecoanet et *al.*, 1999), measures were achieved in the “Pin-mode” of the kappameter which takes into account a geometric factor to reduce roughness effects.

About 4050 magnetic susceptibility measurements were taken directly on 130 outcrops, all along the southeastern border of the Armorican Massif and the northwestern border of the Massif Central and Poitou High (Fig. 3a). Within each litho-structural unit, most of the outcropping lithologies were sampled. The compilation of these measurements is presented in Fig. 5. For each litho-structural unit, we numerated the magnetic susceptibility measurements within constant intervals of variation. In Fig. 5, the colored bars highlight the most represented magnetic susceptibility ranges, whereas the grey intervals indicate ranges with few randomly distributed data.

As an aid for the interpretation, the magnetic susceptibility was subdivided into three representative ranges, based on the classification of Clark and Emerson (1991) and the separation range of Théveniaut and Clarke, (2013): i) from negative values to 4 x 10-4 SI, ii) from 4 x 10-4 to 5 x 10-3 SI and iii) above 5 x 10-3 SI, designated as low, intermediate and high magnetic susceptibility ranges, respectively. Fe-rich sandstones in Central Brittany exhibit the highest magnetic susceptibility of the study area (Fig. 5). Basic rocks (gabbro-diorite, granodiorite and amphibolite), and Cambrian felsic volcanites are also within the high magnetic susceptibility range, due to their high amount of ferrimagnetic minerals, such as magnetite, in their mineralogical composition (Thiéblemont et *al.*, 2011). Granite, leptynite, orthogneiss, migmatite, Neoproterozoic metasedimentary and Paleozoic sedimentary rocks, micaschists and metasediments are within the low magnetic susceptibility range, given that they are mainly composed of diamagnetic (quartz, plagioclase) and paramagnetic minerals. Some Paleozoic sedimentary rocks, basalts, metabasites, meta-gabbro, diorites and amphibolites are within the intermediate range, since they contain paramagnetic minerals, and a small amount of iron-bearing minerals (amphibole, biotite or clay minerals).

Induced magnetization is predominant in the area, but several bimodal anomalies in the RTP map (Fig. 3b) indicate some remnantly magnetized rocks. To the north, the Fe-rich Ordovician sandstones of Central Brittany, mainly composed of magnetite, have been studied in detail (Corpel and Weber, 1970): their Koenigsberger ratio is around 6 but the remnant component of magnetization is almost collinear to the ambient magnetic field and therefore does not strongly affect the mapping of this unit. Also, the granodiorite within the Choletais area and the diorite plutons within the Confolentais area are partly remnantly magnetized, but their magnetic anomalies almost perfectly match their field cartographic limits (Fig. 3b). This suggests that i) the effect of the remnant magnetization is weak, or ii)

307 their direction of remnant magnetization is close to the induced magnetization. In these
308 three cases, the location of the magnetic causative bodies is only slightly affected by the
309 remnant magnetization and these lithologies also display a high magnetic susceptibility in
310 the field (Fig. 5). Consequently, we made the assumption that the interpretation of the
311 magnetic maps could be achieved considering the magnetic susceptibility only.
312 Globally, there is a significant overlap between the magnetic susceptibility ranges of the
313 various lithologies; however, this overlap is rather limited between lithologies within each
314 litho-structural unit. This observation is crucial for the geophysical maps interpretation, as
315 described in the following paragraphs.

316 ***4.2 Density***

317 Density is the petrophysical property influencing the gravity data. For this study, 54
318 unweathered rock samples from most of the lithologies were collected all along the
319 Armorican and Massif Central borders in 48 outcrops (Fig. 3a). The densities of these
320 samples were measured using the double weighting method, with a ca. 0.01 g/cm^3
321 uncertainty. The density determination of some lithologies was not possible due to bad
322 outcropping conditions. In this case, a density value was affected with respect to the density
323 average of the same lithology in the other litho-structural units.
324 As for the magnetic susceptibilities, the densities were subdivided into three representative
325 groups: i) from 2.55 to 2.65 g/cm^3, ii) from 2.65 to 2.8 g/cm^3, and iii) above 2.8 g/cm^3 for
326 low, intermediate and high densities, respectively (e.g. Edel, 2008) (Fig. 5).

327

328 **5. Geophysical signatures of the Paris Basin substratum**

329 The previous studies investigating the substratum of the Paris Basin using magnetic and
330 gravity data manually outlined the main geophysical anomalies. They were interpreted with
331 simplified lithological attributions, based on the substratum nature documented in some
332 boreholes as well as some rock property data (Weber, 1973; Debeglia and Weber, 1980).
333 More recently, Martelet et *al.*, (2013) proposed a map of petrophysical signatures of the
334 substratum of the south-central part of the Paris Basin, based on a numerical classification
335 combining gravity and magnetic data. We used the same approach to achieve a simplified
336 magnetic-gravity signature of the substratum of the study area.
337 We agree with previous studies that considered the magnetic effect of the Meso-Cenozoic
338 sedimentary cover of the Paris Basin, almost “transparent” for the magnetic field
339 (Weber, 1973); therefore the magnetic map mostly features the buried substratum.
340 Nevertheless the Meso-Cenozoic sedimentary pile at least attenuates the intensity of the
341 magnetic response of the substratum and increases the wavelength of the substratum
342 anomalies, as the sedimentary cover gets thicker; from 0 to about 2000m in the study area.
343 The gravity field contains both the effects of the substratum and of the sedimentary basin.
344 The vertical gradient of the Bouguer anomaly used for our classification attenuates the long
345 wavelengths of the Meso-Cenozoic sedimentary pile (Debeglia and Weber 1985; Martelet
346 et *al.*, 2013). Aiming at the same goals as Martelet et *al.*, (2013), the map of the magnetic
347 anomaly reduced to the pole that was introduced in our classification, followed two
348 considerations: 1) displaying information of the structure and magnetization of the
349 substratum as detailed as possible; 2) being physically as homogeneous as possible with
350 the gravity first vertical derivative. We added a third consideration: 3) reducing as much as
351 possible the variable smoothing and attenuating effect of the Meso-Cenozoic sedimentary
352 pile. Combining the characteristics of RTP and the TILT fulfils the three conditions. These
353 two magnetic maps were combined with the vertical gradient of the Bouguer anomaly to

obtain synthetized signatures of magnetic and gravity data. The three layers were combined into a ternary image, using a standard image fusion procedure. We then performed a numerical classification of this ternary image using unsupervised isodata clustering (e.g. Venkateswarlu and Raju, 1992). Based on their gravity and magnetic signatures, all pixels of the map were statistically distributed among 6 classes (Fig. 6a) which well figure the geophysical signatures of the outcropping geology. This map displays self-consistent cartographic bodies, which are compatible with known geological patterns. It features 2 levels of magnetic intensity (from light to dark green) and an intermediate average magnetic/gravity signature (in white) as well as 3 levels of gravity intensity (from light to dark blue). These synthetized geophysical signatures can be related to the simplified 3-levels categorization of the petrophysical magnetization/density parameters (Fig. 5). This map combines magnetic and gravity signatures and it is used as a support for the following structural and lithological interpretations.

6. Geological map of the pre-Mesozoic substratum

The first step of the interpretation consists in extending below the Paris Basin sedimentary cover the major structures recognized in the field (Fig. 2a) in order to delineate the Variscan litho-structural units under cover. The structural interpretation (Fig. 6b) uses all geophysical enhanced maps presented in Section 3 supported by the synthetized geophysical signatures map (Fig. 6a). The second step consists in interpreting the lithological nature of the hidden substratum, using the combined petrophysical characteristics of rocks (Fig. 5), the synthetized geophysical signatures of the substratum (Fig. 6a) and the structural sketch map including available boreholes (Fig. 6b).

6.1 Undercover delineation of structural features

Manually interpreted geophysical trends deriving from the magnetic and gravity maps are outlined in red in Fig. 6a. They underline the N110E-N120E and N90E striking structural directions of the Armorican Massif and the Massif Central, respectively, known in the field. In addition to these trends, main geophysical structures and discontinuities were interpreted. The interpretative structural map (Fig. 6b) showing the extension of the structural units below the Paris Basin cover is discussed from north to south.

Central Brittany is limited to the north by the NASZ. Its extension constitutes the northern limit of the study area; it is defined regionally by a major N110°E-oriented disharmony between the strong magnetic signals of Central Brittany to the south, and the northern weak magnetic signals (Fig. 3b). It also outlined by a successive E-W striking chaplet of magnetic anomalies bounded the NASZ to the north, which can be outlined from the field to the easternmost part of the studied area (Baptiste et *al.*, 2015) (Fig. 3c, Fig. 3d). The Lanvaux unit is marked by a well-defined NW-SE striking elongated low density anomaly, known as Lanvaux orthogneiss (Fig. 4b); it is bounded to the north by the NBSASZ. Following the magnetic and gravity trends under cover (Fig. 6a), the strike of the NBSASZ changes eastwards from NW-SE to NE-SW and joins the NASZ, limiting Central Brittany to the east (Fig. 6b). The southern border of the noticeable Lanvaux low gravity anomaly defines the limit between the Lanvaux unit and the northern part of St-Georges-sur-Loire unit (Fig. 6b).

In the field, the St-Georges-sur-Loire unit is characterized by low magnetic (Fig. 3b) and gravity signal (Fig. 4b), and by scattered moderate intensity magnetic anomalies (Fig. 3c) and a high intensity gravity anomaly, to the north and south, respectively. Predominant NW-SE/E-W striking geophysical trends are also observed (Fig. 6b). Under the Paris Basin sedimentary cover, the northern and southern part cannot be separated by geophysical data. The southern border of the high intensity gravity anomaly defines the southern limit of

402 the St-Georges-sur-Loire unit (Fig. 4b); it defines the cartographic trace of the NSE
403 Eo-Variscan suture (Fig. 6b).
404 The Choletais area, marked by an E-W striking high gravity elongated anomaly, extending
405 150km eastwards below the Paris Basin sedimentary cover (Fig. 4b), is bounded to the
406 south, by the northern branch of the Cholet fault (Fig. 6b). This noticeable anomaly defines
407 the southward boundary of the Mauges nappe. Along this fault, the magnetic and gravity
408 trends strike E-W in continuity along more than 150 km (Fig. 6a). Northwards, the
409 geophysical trends become less and less continuous (Fig. 6a), suggesting the decreasing
410 gradient of deformation away from the fault, as observed in the Armorican Massif
411 (Thiéblemont et *al.*, 2011). To the east (around 2°E), the E-W striking Cholet fault marks the
412 northern limit of NW-SE geophysical trends of the Aigurande Plateau. Altogether, these
413 features suggest that the Cholet fault can be considered as a major shear zone.
414 In the east of the study area (around 2°E), the NSE fault and the northern branch of the
415 Cholet fault almost meet, closing the Mauges nappe and the Choletais area, to the east
416 (Fig. 6a). To the south of the Cholet fault, low gravity anomalies (Fig. 4b) and signatures
417 (Fig. 6a) and NW-SE striking geophysical trends (Fig. 6a) are predominant; this refers to
418 the Haut Bocage unit and Confolentais area connection. To the east of the Haut Bocage
419 unit, the direction of geophysical trends progressively changes from NW-SE to E-W,
420 featuring the connection between the Haut Bocage unit and Aigurande Plateau.
421 In the easternmost part of the studied area, all these units are interrupted by NE-SW
422 striking structures bounding the Permo-Carboniferous Contres basin, well characterized on
423 seismic profiles and in deep boreholes (Fig. 6b; Beccaletto et *al.*, 2015).
424 At the regional scale, all structures are offset by N150E-N160E-striking faults and, to a
425 lesser extent, by their conjugate N20E-N30E striking faults (Fig. 6b). In agreement with
426 Martelet et *al.*, (2013), two kinematics are interpreted along the N150E-N160E faults: i) a

427 dextral motion highlighted by the offset of preexisting structures and lithological markers,
428 and ii) a vertical movement documented by the attenuation and the spreading of the
429 magnetic signal from west to east. In the southeastern part of the Armorican Massif, the
430 N150E striking Partenay fault is described as a middle to upper Visean dextral shear zone
431 (Rolin et *al.*, 2009). The seismic information confirms the role of these faults during the
432 opening of Carboniferous or Permian Arpheuilles and Contres basins (Fig. 6b; Beccaletto et
433 *al.*, 2015). Moreover, they were interpreted as Permian or Triassic fracture zones
434 reactivated during the opening of the North Atlantic Ocean and Gulf of Biscaye (Vigneresse,
435 1988). They are also known throughout the Armorican Massif, where they bound small
436 Tertiary basins. Based on these information, the N150E-N160E striking faults can be
437 interpreted as Variscan faults, reactivated during the tectonic evolution of the Paris Basin,
438 strongly affecting present-day geometry in the southwestern part of the basin.
439 The N30E striking normal faults, mainly located in the Mauges nappe (Fig. 6b), are also
440 interpreted as Variscan structures reactivated during the Permo-Carboniferous, controlling
441 the geometry of the Arpheuilles basin (Fig. 6b; Beccaletto et *al.*, 2015).

442 ***6.2 Interpretation of the undercover lithologies***

443 Based on the geophysical signatures and the structural information, we propose a
444 geological map displaying the interpreted lithologies assigned to the dominant geophysical
445 signatures (Fig.7a) and an interpretative cross section based on geological information
446 observed in the field (Fig. 7b). This geological map as well as its tectonic implications are
447 discussed in each litho-structural unit.

448 ***6.2.1 Central Brittany***

449 Central Brittany is mainly composed of Neoproterozoic metasedimentary rocks and
450 Paleozoic sedimentary rocks intruded by Carboniferous granites (Fig. 2). In this

451 litho-structural unit, high magnetization and density signatures (Fig. 6a) unambiguously
452 refer to the Fe-rich Ordovician sandstone (up to 0.8 SI and 3.11 g/cm^3; Fig. 5). This marker
453 extends eastwards, bounding the NBSASZ (Fig. 8a); its presence is confirmed at 300m
454 depth under cover by a borehole (Fig. 6b).
455 Contrary to previous models (Weber, 1971, 1973; Debeglia and Weber, 1980), the
456 Paleozoic rocks can be discriminated from the Neoproterozoic ones using the petrophysical
457 information. Paleozoic rocks including Fe-rich sandstones displaying low magnetization and
458 density (from 1.5 to 5 x 10^{-4} SI and 2.71 g/cm^3; Fig. 5) can be traced eastwards (Fig. 7a). In
459 the field, geophysical signatures of the Neoproterozoic metasedimentary rocks are
460 heterogeneous, with intermediate magnetic susceptibility and low density (from 10^{-4} to
461 3 x 10^{-4} SI and 2.55 g/cm^3; Fig. 5). They are also intruded by moderately magnetic and
462 dense (3.11 g/cm^3) gabbroic dykes (Verhnet et *al.*, 2009). Thus the map exhibits a
463 succession of thin E-W trends with intermediate to high magnetic and intermediate gravity
464 signatures that can be identified under the sedimentary cover and grouped with the
465 Neoproterozoic metasedimentary rocks (Fig. 6a). The Laval basin has intermediate to low
466 magnetic and gravity signatures as well as peculiar E-W trending texture (Fig. 6a) well
467 visible in the magnetic vertical gradient (Fig. 3c). This E-W trending signature is likely
468 related to interbedded basalts with intermediate magnetization and density (up to 10^{-2} SI
469 and 2.85 g/cm^3; Fig. 5) as observed in the field (Fig. 8b). This feature allows delimiting the
470 southern extension of the Laval basin under the Paris Basin cover (Fig. 8b). Furthermore,
471 the low magnetic and gravity signatures (Fig. 6a) are related to Carboniferous granite
472 intrusions (less than 5 x 10^{-4} SI and 2.65 g/cm^3; Fig. 5). Witnesses of these granitic plutons
473 are mapped in the field, bounded and affected by the dextral shearing of the NASZ: the
474 Pertre granite emplaced at 343 ± 3Ma (Verhnet et *al.*, 2009) and the Craon granite (e.g. Le

475 Gall et *al.*, 2011; Trautmann et *al.*, 2011). The location and the shape of the undercover
476 granites suggest that they probably are affected by the NASZ shearing (Fig. 8c).
477 Overall, the Central Brittany litho-structural unit, delimited to the south by clear markers of
478 Fe-rich Ordovician sandstones, appears also limited to the east, at the junction between the
479 NASZ and the NBSASZ (Fig. 6b). In the southwestern part of the Paris Basin, these
480 interpretations are consistent with the tectonic sketch of major Armorican shear zones
481 proposed by Martinez Catalàn et *al.*, (2012). The southern part of Central Brittany is
482 structured by patterns of Neoproterozoic and Paleozoic sedimentary rocks. In its
483 northwestern part, the early-Carboniferous Laval basin is developed along the NASZ; it is
484 delimited by low magnetic and gravity signatures (Fig. 6b) related to granitic bodies (Fig.
485 7a), to the south.

486

487 ***6.2.2 The Lanvaux unit***

488 In agreement with previous works, the eastern extension of the Lanvaux negative gravity
489 anomaly (Fig. 4b) is well documented along more than 200 km (Weber, 1973; Debeglia and
490 Weber, 1980; Autran et *al.*, 1994; Martelet et *al.*, 2013). This anomaly is interpreted as
491 deriving from the low magnetization and low density signatures of the Lanvaux orthogneiss,
492 confirmed by the petrophysical measurements (from 10^{-5} to 0.7×10^{-4} SI and 2.55 g/cm^3;
493 Fig. 5). In the field, the Carboniferous Bécon and the St-Lambert granites display low
494 magnetic susceptibilities and densities comparable to those of the orthogneiss (from $2 \times$
495 10^{-5} to 10^{-4} SI; Fig. 5); it is therefore not possible to discriminate the older Lanvaux
496 orthogneiss (477 ± 18 Ma; Guerrot et al., in Janjou et *al.*, 1998) from the Carboniferous
497 granites. The Carboniferous granites being mainly located along the SBSASZ (Fig. 8c), we
498 consider that the low magnetic and gravity signatures are related to the Lanvaux

499 orthogneiss (Fig. 8c). Eastwards, under cover, the strike of the NW-SE Lanvaux
500 orthogneiss evolves to an E-W and progressively NE-SW direction, parallel to the NBSASZ
501 (Fig. 8c). Lanvaux unit is an antiform (Faure and Cartier, 1998), with Neoproterozoic
502 metasedimentary and Paleozoic sedimentary rocks similar to those of the Central Brittany
503 and with comparable petrophysical characteristics (Fig. 5). The succession of geophysical
504 signatures of metasedimentary and sedimentary rocks as well as the orthogneiss observed
505 in the field extends eastwards under the Paris Basin sedimentary cover. This suggests that
506 the unit has the same antiformal structure, throughout its eastward extension (Fig. 7b). At
507 the southern border of the Lanvaux unit, the magnetic signature of the Paleozoic rocks
508 highlights the tectonic limit with the St-Georges-sur-Loire unit (Fig. 6b).

509

510 ***6.2.3 The St-Georges-sur-Loire unit***

511 Whereas cartographically well marked under cover, the eastern extension of the St-
512 Georges-sur-Loire unit has various geophysical signatures (Fig. 6a), rather magnetic and
513 dense. Cartographically, these signatures cannot be formally related to the
514 northern/southern parts of the unit, as observed in the field (Fig. 2a). The northern part of
515 the unit is marked by low magnetic and gravity signatures (Fig. 6a) related to a granitic
516 pluton (up to 10^{-4} SI and 2.65 g/cm^3; Fig. 5), located at the junction between the Lanvaux
517 and the St-Georges-sur-Loire units, mostly hidden below the Paleozoic series (up to 5 x 10^{-}
518 ^{4} SI and 2.68 g/cm^3). Granites located along the SBSASZ (Fig. 8c) belong to a leucogranite
519 belt displaying dextral shearing, associated with the emplacement of the leucogranite
520 plutons (Berthé et *al*., 1979; Jégouzo, 1980; Vigneresse and Brun, 1983; Gapais et *al*.,
521 1993; Turillot et *al*., 2009). Among them, Questembert and Lizio leucogranites (Fig. 8c)
522 emplaced at 316 ± 3 Ma and 316 ± 6 Ma (Tartèse et *al*., 2011b, 2011a), in agreement with

523 the St-Lambert granite located to the Lanvaux unit, which displays S/C structures
524 suggesting an emplacement during the dextral shearing of the NBSASZ at 312 ± 3 Ma
525 (Faure and Cartier, 1998). Under cover, these low magnetic and gravity signatures are not
526 observed (Fig. 6a), thus these granites cannot be extended eastward, suggesting a limited
527 eastward extension of the leucogranitic belt.
528 The southern part of the unit, the blocky sub-unit is characterized by scattered high
529 magnetic and various low to high gravity signatures (Fig. 6a). Below the Paris Basin
530 sedimentary cover, the high magnetic and gravity signatures elongated eastwards
531 throughout the map, likely correspond to basic rocks, as interpreted by Martelet et *al.*,
532 (2013). These basic rocks can be variously interpreted in terms of lithology: i) basaltic or
533 gabbroic olistostoliths as described in this unit in the Armorican Massif (Cartier and Faure,
534 2004), ii) interbedded basalts related to the opening of a back-arc basin (Ducassou et *al.*,
535 2011) or iii) mafic rocks such as the ophiolites which sporadically crop out along the NSE
536 fault (Marchand, 1981; Faure et *al.*, 2008; Ballèvre et *al.*, 2009). In the eastern part of the
537 St-Georges-sur-Loire unit, the depth of the contact between the substratum and the
538 sedimentary cover is defined at about 500 m, and the bodies responsible for the magnetic
539 signal are located at more than 1500 m depth (Martelet et *al.*, 2013). Consequently the
540 magnetic susceptibility of the magnetic source has to be strong enough to produce such a
541 magnetic signature. According to the magnetic susceptibility measured in the field in St-
542 Georges-sur-Loire unit, we cannot interpret the source as basalts since they do not yield a
543 high magnetic susceptibility (from 6 to 8 x 10^{-4} SI; Fig. 5). The third hypothesis better
544 complies with the petrophysical signatures and with other evidence reported in the
545 literature. Indeed, the interpretation of the Armor2 seismic profile, located in the southern
546 part of the Armorican Massif (Bitri et *al.*, 2003), suggested the presence of the northern part
547 of the Champtoceaux complex beneath St-Georges-sur-Loire unit. The northern part of this

548 complex crops out as ophiolitic series along the NSE fault; it is made of high magnetic
549 susceptibility and high density rocks, such as amphibolite, and micaschists (from 1.1 to 1.5
550 x 10^{-2} SI, 3.02 g/cm^3 and up to 0.3 SI, 2.79 g/cm^3, respectively; Fig. 5). Therefore, contrary
551 to previous sketch (Weber, 1973; Debeglia and Weber, 1980), our results reveal the
552 eastward extension of ophiolitic series marking the NSE Eo-Variscan suture (Fig. 8d); it is
553 supported by high magnetic and gravity signatures which extend up to the eastern part of
554 the study area limiting St-Georges-sur-Loire unit to the south.

555

556 ***6.2.4 The Mauges nappe and the Champtoceaux Complex***

557 The Mauges nappe, mainly composed of Neoproterozoic micaschists (Fig. 2), exhibits both
558 low magnetic and gravity signatures (Fig. 6a) that may account for hidden granitic plutons.
559 Granitic rocks crop out locally, as for instance the Chemillé pluton intruding the Mauges
560 micaschists, displaying low magnetic susceptibility and density (up to 8 x 10^{-4} SI and
561 2.55 g/cm^3; Fig. 5). Similar low geophysical signatures depicted in the undercover
562 extension of the Mauges nappes (Fig. 6a) suggest the presence of punctual granitic
563 plutons, probably similar to the Chemillé granite (Fig. 8c). Also, metabasites interbedded in
564 the micaschists yield higher magnetic susceptibility and density ranges (from 5 to 7 x 10^{-4}
565 SI and 2.82 g/cm^3; Fig. 5) than the surrounding micaschists. These signatures trace the
566 eastward extension of the Mauges nappe under the sedimentary cover of the southern part
567 of the Paris Basin (Fig. 7a).
568 The Choletais area is composed of Cambrian acidic volcanites, intruded by microgranite,
569 granodiorite and gabbro-diorite, unconformably covering the Neoproterozoic rocks (Fig. 2).
570 Among them, the Vézins granodiorite (Fig. 8c) emplaced at 345 ± 5 Ma (Thiéblemont et *al*.,
571 2011) is supposed to be a syn-kinematics intrusion related to the dextral shearing of the

572 Cholet fault (Rolin et *al*., 2009). In the Choletais area, the magnetic susceptibilities and
573 density measurements do not discriminate the gabbro-diorite suites from the granodioritic
574 plutons (from 4 to 7 x 10^{-2} SI, 2.83 g/cm^3 and from 2 to 5 x 10^{-2} SI, 2.73 g/cm^3, respectively;
575 Fig. 5). For this reason, these lithologies are grouped together as "basic rocks" in the
576 interpretative geological map (Fig. 7a). The Cambrian volcanics are discrimated by a lower
577 density compared to basic rocks (2.65 g/cm^3 and from 2.73 to 2.83 g/cm^3, respectively; Fig.
578 5). As previously described (Weber, 1971), in the southern part of the Mauges nappe, the
579 northern branch of the Cholet fault is bounded to the north by an unexpected E-W striking
580 high density elongated anomaly, which extends 200 km eastwards (Fig. 4b). It is
581 superimposed, in the Armorican Massif, to the low magnetization and low density Thouars
582 microgranite (from 1 to 7 x 10^{-4} SI and 2.65 g/cm^3; Fig. 5). The high intensity anomaly can
583 however be explained by the close association of acidic and basic magmatism composing
584 the Thouars massif (Mathieu, 1943, 1958; Weber, 1971) emplaced at 519 ± 10 Ma
585 (Thiéblemont, et *al*., 2011). The high resolution geophysical data enhance this dual
586 anomaly: it highlights punctual high magnetization signatures associated with high density
587 anomaly (Fig. 6a) related to basics rocks (from 3 to 6 x 10^{-2} SI and up to 2.83 g/cm^3; Fig. 5)
588 and the presence of high density intrusive dolerite (2.97 g/cm^3; Fig. 5) located along the
589 Cholet fault, at the junction between the Mauges nappe and the Haut Bocage unit.
590 The early Carboniferous Ancenis basin is marked by a low gravity anomaly (Fig. 4b) likely
591 related to a hidden granitic pluton (Fig. 8c) as previously described by Martelet et *al.*, (2013)
592 as well as E-W striking high magnetic trends well defined in the vertical gradient of the
593 magnetic anomaly. This contrast can reasonably be related to the northern extension of the
594 Champtoceaux complex, corresponding to the ophiolitic nappe, buried below the Ancenis
595 basin, along the NSE fault, also interpreted in Armor2 seismic profile (Bitri et *al.*, 2003).

596 Following the NSE fault to the east, the Permo-Carboniferous Arpheuilles basin, recognized
597 by seismic profiles under cover (Beccaletto et *al.*, 2015) and two boreholes (Fig. 6b),
598 exhibits a peculiar texture in the magnetic first vertical derivative (Fig. 3c) and tilt (Fig. 3d)
599 maps. This texture allows delimiting the extension of the Arpheuilles basin (Fig. 8b).
600 Superimposed on the magnetic texture, high intensity magnetic anomalies are interpreted
601 as the presence of Cambrian volcanic rocks (Fig. 7a) underlying Arpheuilles basin,
602 accompanied by granitic plutons highlighted by their low gravity signatures (Fig. 6a). Our
603 results show that, to the north, Arpheuilles basin is bounded by the NSE fault and controlled
604 by N150E striking faults as well as their N30E-N40E conjugates (Fig. 8b). This suggests
605 that the Arpheuilles basin may be the lateral equivalent of the early Carboniferous Ancenis
606 basin.

607

608 ***6.2.5 The Aigurande Plateau and its connection with the Haut Bocage unit***

609 This area consists in a stack of metamorphic nappes intruded by granitic plutons (Fig. 2).
610 Under cover, the Cholet fault delimits the northern contact of the high grade metamorphic
611 nappes with the Mauges nappe, composed of low grade micaschists (Fig. 8d).
612 In the northern part of the Aigurande Plateau, the Lower Gneiss Unit (LGU), is mainly
613 composed of low magnetic susceptibility and density micaschists and metagrauwackes (up
614 to 4×10^{-4} SI and 2.8 g/cm^3; Fig. 5), and intermediate magnetic and high density
615 amphibolite (from 5 to 9 x 10^{-4} SI, 3.01 g/cm^3). The Upper Gneiss Unit (UGU) was
616 discriminated from the LGU by both the high magnetic and density signatures (Fig. 6a)
617 deriving from the amphibolites within the leptynite-amphibolite complex (from 1.5 x 10^{-2} to 5
618 x 10^{-2} SI and 2.98 g/cm$^{3;}$ Fig. 5). Consequently, the LGU/UGU contact can be mapped
619 under the Paris Basin sedimentary cover, bounded to the north by the northern branch of

620 the Cholet fault (Fig. 7a). The LGU micaschists are associated with the Haut Bocage unit
621 described in the field (Fig. 6b; Fig. 7a), which consist of a stack of metamorphic nappes,
622 refolded in an ENE-SSW striking antiform/synform succession, intruded by Carboniferous
623 granites (Fig. 7b).
624 The micaschists of the Para-autochtonous unit displaying low to intermediate magnetic
625 susceptibility and density (up to 4 x 10^{-4} SI and 2.68 g/cm^3), related to low to intermediate
626 magnetic and gravity signatures (Fig. 6a), has no characteristic signature that can be
627 mapped under the Paris Basin sedimentary cover.
628 In this area, granitic plutons belong to the Hercynian Mortagne – Marche leucogranites belt
629 (Vigneresse, 1988; Gapais et *al.*, 1993; Vigneresse, 1999; Rolin and Colchen, 2001; Rolin
630 et *al.*, 2009; Edel et *al.*, 2015; Gapais et *al.*, 2015). These granites are largely represented
631 in the Haut Bocage unit and Massif connection (Fig. 7a).

632

633 ***6.2.6 The Poitou High: the Haut Bocage unit and the Confolentais area junction***
634 Largely represented in the field, in the Haut Bocage unit and the Confolentais area
635 (Fig. 6b), the low magnetic and gravity signatures (Fig. 6a) are related to granitic plutons
636 (from 0.8 x 10^{-5} to 10^{-4} SI and 2.65 g/cm^3; Fig. 5). Under cover, equivalent magnetic and
637 gravity signatures related to granitic plutons described in the Poitou High (from 2.5 to
638 4 x 10^{-5} SI and 2.62 g/cm^3; Fig. 5), mark the connection between the southern part of the
639 Haut Bocage unit and Confolentais area (Fig. 7a). As largely recovered in boreholes (Fig.
640 6b), granitic plutons represent the main rocks of the substratum in this area (Fig. 7a). These
641 granitic plutons consist in leucomonzogranites, leucogranites, granodiorites and calk-
642 alkaline diorites. They belong to a granitic belt emplaced from late Devonian to early-
643 Carboniferous and are associated with the shearing of the various branches of the SASZ

644 (see Rolin et al., 2009 for more information). Using the geophysical signatures of the
645 substratum (Fig. 6a), it is not possible to discriminate the various leucomonzogranites,
646 leucogranites and granodiorites.
647 Under the sedimentary cover, the southern part of the Poitou High is marked by punctual
648 high magnetic and gravity signatures (Fig. 6a) related to the calk-alkaline diorite plutons
649 exposed in the field, both in Confolentais area and Haut Bocage unit (Fig. 6b). These diorite
650 plutons emplaced at 373 ± 10 Ma (Cuney et al., 1993) and from 360 ± 3 Ma to 349 ± 5 Ma
651 (Bertrand et al., 2001; Alexandre et al., 2002) for the Montcoutant and various Poitou High
652 diorite plutons, respectively, are associated with the dextral shearing of the SBSASZ (Fig.
653 8c) (see Rolin et al., 2009 for more information). In the southern Aigurande Plateau, Huriel
654 diorite intrusion (Fig. 8c) emplaced at 361 ± 1 Ma (Pin and Paquette, 2002) and post-date
655 the dextral shearing of the Marche fault (Rolin et al., 2009). Diorite plutons have consistent
656 high magnetic susceptibility and density (up to 1.5 x 10^{-2} SI and 2.80 g/cm^3 and from 3 to 6
657 x 10^{-3} SI, and 2.80 g/cm^3, respectively; Fig. 5). These basic rocks are discriminated i) from
658 the intermediate magnetic and low density signatures corresponding to the LGU host
659 micaschists, in the Haut Bocage unit, and ii) from the high magnetic and intermediate
660 signatures related to the metavolcanites belonging to the UGU (up to 0.3 SI; Fig. 5), in the
661 Confolentais area (Fig. 7a).

662

663 ## 7. Summary and Conclusion

664 Our paper outlines the benefit of a joint interpretation of potential fields (high-resolution
665 aeromagnetic and gravity data) and petrophysical characterization (magnetic susceptibility
666 and density measurements on rock samples), in order to derive reliable lithological and
667 structural mapping of a buried substratum.

In order to propose a geological map of the hidden substratum of the southwestern part of the Paris Basin, our methodology, is divided into five successive stages: i) the potential field data were processed, with the aim to get specific information (geophysical contrasts, structural features…), ii) magnetic susceptibilities and densities were measured on field rock samples along the eastern border of the Armorican Massif and the northern border of the Massif Central, leading to a petrophysical library of lithologies, iii) using selected magnetic and gravity maps, a map of geophysical signatures was synthetized using an unsupervised classification, featuring 6-levels of magnetic/gravity intensities, iv) the combined analysis and interpretation of magnetic and gravity trends with the synthetized geophysical signatures, allowed extending the Variscan litho-structural units below the Paris Basin sedimentary pile, v) relating the geophysical signatures to the petrophysical characteristics (density and magnetization) within each litho-structural unit, allowed interpreting a geological map of the substratum. This updated study reveals new geological information: i) the limited eastward extension of Central Brittany, bordered to the east by the NE-SW striking NBSASZ; ii) the eastward extension, along ca. 150 km, of the Cholet fault, interpreted as a major fault, delineating the northern limit of the Aigurande Plateau; iii) the emphasis on a series of N150E-N160E and N30E striking normal Variscan fault, reactivated during the tectonic history of the Paris Basin, especially controlling the opening of Permo-Carboniferous basins; iv) the extension of the Nort-sur-Erdre fault considered as an ophiolitic suture, documented by the presence of high magnetic and density rocks along the southern part of the St-Georges-sur-Loire unit.

Overall, our methodology provides keys for extensive mapping of buried basement using magnetic, gravity and petrophysical data. In the near future, this study will be extended to the entire Paris Basin in order to propose a complete geological map of the pre-Mesozoic substratum of the Paris Basin.

Acknowledgments

This work is part of a PhD Thesis co-funded by Région Centre and BRGM. We thank an anonymous reviewer and J.B. Edel for useful and constructive comments, which contributed to improving the manuscript. Geophysical maps were drawn using Geosoft© software.

References

Alexandre, P., Le Carlier de Veslud, C., Cuney, M., Ruffet, G., Virlogeux, D., Cheilletz, A., 2002. Datation 40Ar/39Ar des leucogranites sous couverture du complexe plutonique de Charroux–Civray (Vienne). Comptes Rendus Geoscience 334, 1141–1148. doi:10.1016/S1631-0713(02)01859-X

Autran, A., Lameyre, J., 1980. Conclusions générales. Les granitoïdes de France. Mémoires BRGM 107, 87–99.

Autran, A., Lefort, J.P., Debeglia, N., Edel, J.B., Vigneresse, J.L., 1994. Gravity and Magnetic Expression of Terranes in France and Their Correlation Beneath Overstep Sequences, in: Chantraine, J., Rolet, J., Santallier, D.S., Piqué, A., Keppie, J.D. (Eds.), Pre-Mesozoic Geology in France and Related Areas, IGCP-Project 233. Springer Berlin Heidelberg, pp. 49–72.

Ballèvre, M., Pinardon, J.-L., Kienast, J.-R., Vuichard J.-P., 1989. Reversal of Fe-Mg partitioning between garnet and staurolite in eclogite-facies metapelites from the Champtoceaux nappe (Brittany, France). Journal of Petrology 30, 1321–1349.

Ballèvre, M., Paris, F., Robardet, M., 1992. Corrélations ibéro-armoricaines au Paléozoïque : une confrontation des données paléobiogéographiques et tectonométamorphiques. Comptes Rendus de l'Académie des sciences. Série 2,

717 Mécanique, Physique, Chimie, Sciences de l'univers, Sciences de la Terre 315, 1783–
718 1789.
719 Ballèvre, M., Marchand, J., Godard, G., Goujou, J.-C., Christian, J., Wyns, R., 1994.
720 Eo-Hercynian Events in the Armorican Massif, in: Chantraine, J., Rolet, J., Santallier,
721 D.S., Piqué, A., Keppie, J.D. (Eds.), Pre-Mesozoic Geology in France and Related
722 Areas, IGCP-Project 233. Springer Berlin Heidelberg, pp. 183–194.
723 Ballèvre, M., Lardeux, H., 2005. Signification paléoécologique et paléogéographique des
724 bivalves du Carbonifère inférieur du bassin d'Ancenis (Massif armoricain). Comptes
725 Rendus Palevol 4, 109–121. doi:10.1016/j.crpv.2004.11.011.
726 Ballèvre, M., Bosse, V., Ducassou, C., Pitra, P., 2009. Palaeozoic history of the Armorican
727 Massif: Models for the tectonic evolution of the suture zones. Comptes Rendus
728 Géoscience 341, 174–201. doi:10.1016/j.crte.2008.11.009.
729 Baptiste, J., Martelet, G., Faure., Beccaletto, L., Perrin, J., 2015. Up-to-date regional gravity
730 and aeromagnetic data to unravel the geological patterns of the pre-Mesozoic
731 substratum of the Paris Basin. Variscan 2015 : The Variscan belt : correlations and
732 plate dynamics, Jun 2015, Rennes, France.
733 Beccaletto, L., Hanot, F., Serrano, O., Marc, S., 2011. Overview of the subsurface structural
734 pattern of the Paris Basin (France): Insights from the reprocessing and interpretation of
735 regional seismic lines. Marine and Petroleum Geology, Thematic Set on the
736 Implications of basin dynamics on petroleum systems 28, 861–879.
737 doi:10.1016/j.marpetgeo.2010.11.006
738 Beccaletto, L., Capar, L., Serrano, O., Marc, S., 2015. Structural evolution and sedimentary
739 record of the Stephano-Permian basins occurring beneath the Mesozoic sedimentary
740 cover in the southwestern Paris basin (France). Bulletin de la Société Géologique de
741 France. 6, 429-450.

742 Bernard-Griffiths, J., Peucat, J.J., Sheppard, S., Vidal, P., 1985. Petrogenesis of Hercynian
743 leucogranites from the southern Armorican Massif: contribution of REE and isotopic (Sr,
744 Nd, Pb and O) geochemical data to the study of source rock characteristics and ages.
745 Earth and Planetary Science Letters 74, 235–250. doi:10.1016/0012-821X(85)90024-X
746 Berthé, D., Choukroune, P., Jegouzo, P., 1979. Orthogneiss, mylonite and non coaxial
747 deformation of granites: the example of the South Armorican Shear Zone. Journal of
748 Structural Geology 1, 31–42. doi:10.1016/0191-8141(79)90019-1
749 Bertrand, J.M., Leterrier, J., Cuney, M., Brouand, M., Stussi, J.M., Delaperrière, E.,
750 Virlogeux, D., 2001. Géochronologie U-Pb sur zircons de granitoïdes du Confolentais,
751 du massif de Charroux-Civray (seuil du Poitou) et de Vendée. Géologie de la France 1,
752 167–189.
753 Bitri, A., Ballèvre, M., Brun, J.-P., Chantraine, J., Gapais, D., Guennoc, P., Gumiaux, C.,
754 Truffert, C., 2003. Imagerie sismique de la zone de collision hercynienne dans le
755 Sud-Est du Massif armoricain (projet Armor 2/programme Géofrance 3D). Comptes
756 Rendus Géoscience 335, 969–979. doi:10.1016/j.crte.2003.09.002.
757 Blakely, R.J. 1996. Potential Theory in Gravity and Magnetic Applications (Cambridge
758 University Press).
759 Bonijoly, D., Perrin, J., Truffert, C., Asfirane, F., 1999. Couverture géophysique aéroportée
760 du Massif armoricain, magnétisme et radiométrie spectrale. Rapport BRGM R 40471.
761 Bosse, V., Feraud, G., Ruffet, G., Ballèvre, M., Peucat, J.-J., De Jong, K., 2000. Late
762 Devonian subduction and early-orogenic exhumation of eclogite-facies rocks from the
763 Champtoceaux Complex (Variscan belt, France). Geological Journ*al.* 35, 297–325.
764 doi:10.1002/gj.864.

765 Burg, J.-P., 1981. "Tectonique tangentielle hercynienne en Vendée littorale : Signification
766 des linéations d'étirement E-W dans les porphyroïdes à foliation horizontale." Comptes
767 Rendus de l'Académie des Sciences de Paris, 293, 849-854.
768 Cabanis, B., Wyns, R., 1986. Le volcanisme précambrien des Mauges (sud-est du Massif
769 armoricain) et ses caractères géochimiques. Hercynica, Rennes, (II), 1, 71-78.
770 Cartannaz, C., Rolin, P., Le Métour, J., Fabbri, O., 2006. Fammenian–Tournaisian dextral
771 ductile shear in the French Variscan belt. Comptes Rendus Géoscience 338, 214–221.
772 doi:10.1016/j.crte.2005.12.003
773 Cartier, C., Faure, M., Lardeux, H., 2001. The Hercynian Orogeny in the South Armorican
774 Massif (Saint-Georges-sur-Loire Unit, Ligerian Domain, France): rifting and welding of
775 continental stripes. Terra Nova. 13, 143–149.
776 Cartier, C., Faure, M., 2004. The Saint-Georges-sur-Loire olistostrome, a key zone to
777 understand the Gondwana-Armorica boundary in the Variscan belt (Southern Brittany,
778 France). Int. J. Earth Sci. 93, 945–958. doi:10.1007/s00531-004-0398-3.
779 Cavet, P., Gruet, M., Pillet, J., 1966. Sur la présence du Cambrien à Paroxides à Cléré-sur-
780 Layon (Maine et Loire) dans le Nord-Est du Bocage vendéen (Massif Armoricain).
781 Comptes Rendus Hebdomadaires des séances de l'Académie des Sciences. 263,
782 1685.
783 Cavet, P., Arnaud, A., Barbaroux, L., Blaise, J., Brossé, R., Chauris, L., Gruet, M., Lardeux,
784 H., Rivière, J.-M., 1970. Carte géologique de la France (1/50000), *feuille Chalonnes-*
785 *sur-Loire* (453), BRGM, Orléans.
786 Cavet, P., Lardeux, H., Philippot, A., 1971. Ordovicien et Silurien aux environs de Montjean
787 et Chalonnes (Maine-et-Loire, Sud-Est du Massif armoricain). Mémoires BRGM 73,
788 199-212.

789 Cavet, P., Arnaud, A., Blaise, J., Brossé, R., Chauris, L., Gruet, M., Lardeux, H., 1976.
790 Carte géologique de la France (1/50000), *feuille Angers* (454), BRGM, Orléans.
791 Chantraine, J., Autran, A., Cavelier, C. and collab., 2003. Carte Géologique de la France au
792 1/1000000^{e}. BRGM (6ème édition), Orléans. France.
793 Chauris, L., and Lucas, G., 1964. Les environs de Bécon-les-Granits (Maine-et-Loire)
794 (Feuille d'Ancenis au 80.000e). Bulletin de la Carte Géologique de France, LX-277
795 25–33.
796 Chauris, L., 1969. Sur un important accident structural dans le Nord-Ouest de l'Armorique.
797 Comptes Rendus de l'Académie des Sciences. 268, 2859–2861.
798 Clark, D., Emerson, D., 1991. Notes on rock magnetization characteristics in applied
799 geophysical studies. Exploration Geophysics 22, 547–555. doi:10.1071/EG991547.
800 Corpel, J., Weber, C., 1970. Contribution de l'étude de l'aimantation rémanente à la
801 gîtologie du synclinal ferrifère de Segré. Rapport BRGM/70-SGN-029-GPH, 23 pp.
802 Cuney, M., Stussi, J.-M., Brouand, M., Dautel, D., Michard, A., Gros, Y., Poncet, D.,
803 Bouton, P., Colchen, M., Vervialle, J.-P., 1993. Géochimie et géochronologie U/Pb
804 des diorites quartziques du Tallud et de Moncoutant : nouveaux arguments pour une
805 extension de la Ligne Tonalitique Limousine en Vendée. Comptes Rendus de
806 l'Académie des Sciences. Série 2, Mécanique, Physique, Chimie, Sciences de
807 l'univers, Sciences de la Terre 316, 1383–1390.
808 Dearing, J., 1999. Magnetic susceptibility, in: Environmental Magnetism: A Practical Guide.
809 Quaternary Research Association London, pp. 35–62.
810 Debeglia, N., Weber, C., 1980. Synthèse géologique du bassin de Paris. Mémoires du
811 BRGM n°102.

812 Debeglia, N., Weber, C., 1985. Geologic mapping of the basement of the Paris basin
813 (France) by gravity and magnetic data interpretation. In: The Utility of regional gravity
814 and magnetic anomaly maps, (ed. W.J. Hinze). Society of Exploration Geophysicists.
815 Ducassou, C., Ballèvre, M., Lardeux, H., Robin, C., 2011. Evidence for pre-orogenic, Early
816 Devonian rifting in the Variscan belt: stratigraphy and structure of the Palaeozoic cover
817 of the Mauges Unit (Upper Allochthon, Armorican massif, France). Int. J. Earth Sci.
818 (Geol Rundsch) 100, 1451–1475. doi:10.1007/s00531-010-0605-3.
819 Edel, J.B., 2008. Structure et nature du socle anté-permien du Bassin de Paris d'après les
820 données gravimétriques et magnétiques – Le problème de l'Anomalie Magnétique du
821 Bassin de Paris (AMBP). Géochronique, 105, pp. 31-37.
822 Edel, J.-B., Schulmann, K., Lexa, O., Diraison, M., Géraud, Y., 2015. Permian clockwise
823 rotations of the Ebro and Corso-Sardinian blocks during Iberian–Armorican oroclinal
824 bending: Preliminary paleomagnetic data from the Catalan Coastal Range (NE Spain).
825 Tectonophysics 657, 172–186. doi:10.1016/j.tecto.2015.07.002
826 Elkins, T., 1951. The second derivative method of gravity interpretation. Geophysics. 16,
827 29–50. doi:10.1190/1.1437648.
828 Fairhead, J.D., Salem, A., Cascone, L., Hammill, M., Masterton, S., Samson, E., 2011. New
829 developments of the magnetic tilt-depth method to improve structural mapping of
830 sedimentary basins. Geophysical Prospecting 59, 1072–1086. doi:10.1111/j.1365-
831 2478.2011.01001.x.
832 Faure, M., Prost, A.E., Lasne, E., 1990. Deformation ductile extensive d'age namuro-
833 westphalien dans le plateau d'Aigurande, Massif central francais. Bulletin de la Société
834 Géologique de France VI, 189–197. doi:10.2113/gssgfbull.VI.1.189.
835 Faure M., Leloix C., Roig J.Y., 1997. L'évolution polycyclique de la chaîne hercynienne.
836 Bulletin de la Société géologique de France 168, 695–705.

837 Faure, M., and Cartier, C., 1998. Déformations ductiles polyphasées dans l'antiforme
838 orthogneissique de St-Clément-de-la-Place (unité de Lanvaux, Massif armoricain).
839 Comptes Rendus de l'Académie des Sciences - Series IIA - Earth and Planetary
840 Science 326, 795–802. doi:10.1016/S1251-8050(98)80245-0.
841 Faure, M., Mezeme, E.B., Duguet, M., Cartier, C., Talbot, J.-Y., 2005. Paleozoic tectonic
842 evolution of medio-Europa from the example of the French Massif Central and Massif
843 Armoricain. Journal of the virtual Explorer 19, 1–25.
844 Faure, M., Bé Mézème, E., Cocherie, A., Rossi, P., Chemenda, A., Boutelier, D., 2008.
845 Devonian geodynamic evolution of the Variscan Belt, insights from the French Massif
846 Central and Massif Armoricain. Tectonics 27, TC2005. doi:10.1029/2007TC002115.
847 Faure M., 2014. Le substratum de la France métropolitaine : de la formation du Gondwana
848 à la constitution de la Pangée, une histoire de 600 Ma. Géologues, 180, pp. 13-21.
849 Gapais, D., Lagarde, J.L., Le Corre, C., Audren, C., Jegouzo, P., Casas Sainz, A., Van Den
850 Driessche, J., 1993. La zone de cisaillement de Quiberon: témoin d'extension de la
851 chaine varisque en Bretagne méridionale au Carbonifère. Comptes Rendus de
852 l'Académie des Sciences, Paris, série II 316, 1123–1129.
853 Gapais, D., Brun, J.-P., Gumiaux, C., Cagnard, F., Ruffet, G., Veslud, C.L.C.D., 2015.
854 Extensional tectonics in the Hercynian Armorican belt (France). An overview. Bulletin
855 de la Société Géologique de France 186, 117–129. doi:10.2113/gssgfbull.186.2-3.117
856 Gébelin, A., Brunel, M., Monié, P., Faure, M., Arnaud, N., 2007. Transpressional tectonics
857 and Carboniferous magmatism in the Limousin, Massif Central, France: Structural and
858 40Ar/39Ar investigations. Tectonics 26.
859 Gérard, A., and Griveau, P., 1972. Interpretation quantitative en gravimétrie ou magnétisme
860 à partir de cartes transformées en gradient vertic*al.* Geophysical Prospecting 20, 459–
861 481. doi:10.1111/j.1365-2478.1972.tb00648.x.

862 Goguel, J., and Francia, 1954. Levé gravimétrique détaillé du Bassin parisien. Ministère de
863 l'Industrie et de l'Energie. Direction des Mines. Imprimerie Nationale.
864 Goguel, J., 1972. Tendances modernes dans l'interprétation géologique des données
865 gravimétriques. Bull. BRGM 43–50.
866 Guillocheau, F., Robin, C., Allemand, P., Bourquin, S., Brault, N., Dromart, G., Friedenberg,
867 R., Garcia, J.-P., Gaulier, J.-M., Gaumet, F., others, 2000. Meso-Cenozoic geodynamic
868 evolution of the Paris Basin: 3D stratigraphic constraints. Geodinamica Acta 13, 189–
869 245.
870 Houlgatte, E., Le Hérissé, A., Pelhate, A., Rolet, J., 1988. Evolution géodynamique du
871 Bassin carbonifère de Lav*al.* Géologie de la France 1, 27–46.
872 Jégouzo, P., 1980. The South Armorican Shear Zone. Journal of Structural Geology, Shear
873 zones in rocks 2, 39–47. doi:10.1016/0191-8141(80)90032-2.
874 Lardeux, H., Cavet, P., 1994. Paleozoic of the Ligerian Domain, in: Chantraine, J., Rolet, J.,
875 Santallier, D.S., Piqué, A., Keppie, J.D. (Eds.), Pre-Mesozoic Geology in France and
876 Related Areas, IGCP-Project 233. Springer Berlin Heidelberg, pp. 152–156.
877 Lecoanet, H., Lévêque, F., Segura, S., 1999. Magnetic susceptibility in environmental
878 applications: comparison of field probes. Physics of the Earth and Planetary Interiors
879 115, 191–204. doi:10.1016/S0031-9201(99)00066-7.
880 Le Corre, C., Auvray, B., Ballèvre, M., & Robardet, M., 1991. Le massif
881 armoricain. Scientifical Geological Bulletin. 44, 31-103.
882 Le Gall, J., Vernhet, Y., Lacquement, F., Gauquelin, J.-L., Robert, A., Cocherie, A.,
883 Naveau, J, 2011 – Notice explicative, Carte géologique de France (1/50 000), feuille
884 Laval (319). Orléans : BRGM, 261 p. Carte géologique par Le Gall J., Gigot P.,
885 Savaton P., Lacquement F., Poprawsky Y., Vernhet Y. (2011).

886 Le Hébel, F., Vidal, O., Kienast, J.-R., Gapais, D., 2002. Les « Porphyroïdes » de Bretagne
887 méridionale : une unité de HP–BT dans la chaîne hercynienne. Comptes Rendus
888 Geoscience 334, 205–211. doi:10.1016/S1631-0713(02)01746-7.
889 Le Hérissé, A., and Plaine, J., 1982. Volcanisme basique dans le Carbonifère inférieur du
890 Synclinorium de Laval (Massif armoricain, France). Comptes Rendus de l'Académie
891 des Scences de Paris, 294, 1199-1202.
892 Lienhardt, M.J., 1961. Étude stratigraphique, pétrographique et structurale du socle anté
893 permien du bassin de Paris. Annales de la Société Géologique du Nord 81, 233-241.
894 Marchand, J., 1981. Ecaillage d'un "mélange tectonique" profond: le complexe
895 cristallophyllien de Champtoceaux (Bretagne méridionale). Comptes Rendus de
896 l'Académie des Sciences de Paris 293, 223–228.
897 Martelet, G., Debeglia, N., Truffert, C., 2002. Updating and validating the French gravity
898 terrain corrections out to a distance of 167 km. Comptes Rendus Géoscience. 334,
899 449–454.
900 Martelet, G., Calcagno, P., Gumiaux, C., Truffert, C., Bitri, A., Gapais, D., Brun, J.P., 2004.
901 Integrated 3D geophysical and geological modelling of the Hercynian Suture Zone in
902 the Champtoceaux area (south Brittany, France). Tectonophysics 382, 117–128.
903 doi:10.1016/j.tecto.2003.12.009.
904 Martelet, G., Pajot, G., Debeglia, N., 2009. Nouvelle carte gravimétrique de la France;
905 RCGF09 – Réseau et Carte Gravimétrique de la France, 2009. Rapport BRGM/RP-
906 57908-FR, 77 p.
907 Martelet, G., Perrin, J., Truffert, C., Deparis, J., 2013. Fast mapping of magnetic basement
908 depth, structure and nature using aeromagnetic and gravity data: combined methods
909 and their application in the Paris Basin: Fast mapping of a buried basement using

910 magnetic and gravity data. Geophysical Prospecting 61, 857–873. doi:10.1111/1365-
911 2478.12024.
912 Martínez Catalán J.R., 2012. The Central Iberian arc, an orocline centered in the Iberian
913 Massif and some implications for the Variscan belt. Int. J. Earth Sci. 101, 1299-1314.
914 doi:10.1007/s00531-011-0715-6.
915 Mathieu, G., 1943. Révision de la feuille de Saumur au 1/80000ème. Bulletin du Service de
916 la Carte géologique de France, 212, p119-129.
917 Mathieu, G., 1958. Les grandes lignes de la Vendée. Ibid., 253, 46p.
918 Matte, P., 1986. Tectonics and plate tectonics model for the Variscan belt of Europe.
919 Tectonophysics 126, 329–374. doi:10.1016/0040-1951(86)90237-4.
920 Matte, P., Hirn, A., 1988. Seismic signature and tectonic cross section of the Variscan crust
921 in western France. Tectonics 7, 141–155.
922 Matte, P., 1991. Accretionary history and crustal evolution of the Variscan belt in Western
923 Europe. Tectonophysics 196, 309–337. doi:10.1016/0040-1951(91)90328-P.
924 Mégnien, C., 1980. Synthèse géologique du Bassin de Paris, I, Stratigraphie et
925 paléogéographie, Mémoires du BRGM, 101, 466pp.
926 Miller, H. G. and Singh, V., 1994. Potential field tilt; a new concept for location of potential
927 field sources. Journal of Applied Geophysics. 32, 213–217.
928 Peiffer, M.-T., 1986. La signification de la ligne tonalitique du Limousin. Son implication
929 dans la structuration varisque du Massif Central français. Comptes Rendus de
930 l'Académie des Sciences. Série 2, Mécanique, Physique, Chimie, Sciences de
931 l'univers, Sciences de la Terre 303, 305–310.
932 Perrodon, A. and Zabek, J., 1990. Paris Basin; Interior cratonic basins. AAPG Memoir, 51,
933 633-679.

934 Pin, C., and Paquette, J.-L., 2002. Le magmatisme basique calcoalcalin d'âge dévono-
935 dinantien du nord du Massif Central, témoin d'une marge active hercynienne :
936 arguments géochimiques et isotopiques Sr/Nd. Geodinamica Acta 15, 63–77.
937 doi:10.1016/S0985-3111(01)01079-8.
938 Pomerol, C., 1978. Paleogeographic and structural evolution of the Paris Basin, from the
939 Precambrian to the present day, in relation to neighboring regions. Geologie En
940 Mijnbouw Journal of Geosciences, 57, 533-543.
941 Quenardel, J.-M., Rolin, P., 1984. Palaeozoic evolution of the Plateau d'Aigurande (NW
942 Massif Central, France). Geological Society, London, Special Publications 14, 63–70.
943 doi:10.1144/GSL.SP.1984.014.01.06.
944 Rolin, P., Colchen, M., 2001. Les cisaillements hercyniens de la Vendée au Limousin.
945 Géologie de la France, n° 1-2. 87-116.
946 Rolin, P., Marquer, D., Colchen, M., Cartannaz, C., Cocherie, A., Thiery, V., Quenardel, J.-
947 M., Rossi, P., 2009. Famenno-Carboniferous (370-320 Ma) strike slip tectonics
948 monitored by syn-kinematic plutons in the French Variscan belt (Massif Armoricain and
949 French Massif Central). Bulletin de la Société Géologique de France 180, 231–246.
950 doi:10.2113/gssgfbull.180.3.231.
951 Tartèse, R., Boulvais, P., Poujol, M., Vigneresse, J.-L., 2011a. Granite petrogenesis
952 revealed by combined gravimetric and radiometric imaging. Tectonophysics 501, 98–
953 103. doi:10.1016/j.tecto.2011.02.003
954 Tartèse, R., Poujol, M., Ruffet, G., Boulvais, P., Yamato, P., Košler, J., 2011b. New U-Pb
955 zircon and 40Ar/39Ar muscovite age constraints on the emplacement of the Lizio syn-
956 tectonic granite (Armorican Massif, France). Comptes Rendus Geoscience 343, 443–
957 453. doi:10.1016/j.crte.2011.07.005

958 Taylor, H.L., Mason, M.C., 1972. A Systematic Approach to Well Surveying Calculations.
959 Society of Petroleum Engineers Journal 12, 474–488. doi:10.2118/3362-PA.
960 Théveniaut, H., Clarke, B., 2013. Large scale magnetic susceptibility soil mapping: a proxy
961 for geological mapping and exploration from Bogoso (Ghana). Exploration Geophysics
962 44, 48. doi:10.1071/EG12019.
963 Thiéblemont, D., Cabanis, B., Le Métour, J., 1987. Étude géochimique d'un magmatisme
964 de distension intracontinentale: la série bimodale ordovico-silurienne du Choletais
965 (Massif vendéen), Géologie de la France 1, 65–76.
966 Thiéblemont, D., Guerrot, C., Le Métour, J., Jézéquel, P., 2001. Le complexe de Cholet-
967 Thouars: un ensemble volcano-plutonique cambrien moyen au sein du bloc
968 précambrien des Mauges. Géologie de la France, n°1-2. 7-17.
969 Thiéblemont, D., Augier, R., Ferry, J.-N., Laurent-Charvet, S., Maleyx, C., Ravoux, A.,
970 Lebret, P., Guerrot, C., Chretien, P., 2011 – Notice explicative, Carte géologique de.
971 France (1/50 000), feuille Vihiers (511). Orléans : BRGM, 122 p.
972 Trautmann, F., Lacquement, F., Vernhet, Y., Pivette, B., avec la collaboration de Cocherie
973 A., Guerrot C., Thiéblemont D., Tegyey M., Denis E., 2011. – Notice explicative, Carte
974 géologique de France (1/50 000), feuille Vitré (318). Orléans : BRGM, 131 p. Carte
975 géologique par Lacquement F., Trautmann F., Vernhet Y. (2011).
976 Truffert, C., Gumiaux, C., Chantraine, J., Perrin, J., Galdeano, A., Gapais, D., Ballèvre, M.,
977 Asfirane, F., Guennoc, P., Brun, J.-P., 2001. Levé géophysique aéroporté dans le Sud-
978 Est du Massif armoricain (programme GéoFrance3D Armor2). Magnétisme et
979 radiométrie spectrale. Comptes Rendus de l'Académie des Sciences-Series IIA-Earth
980 and Planetary Science 333, 263–270.

981 Turrillot, P., Augier, R., Faure, M., 2009. The top-to-the-southeast Sarzeau shear zone and
982 its place in the late-orogenic extensional tectonics of southern Armorica. Bulletin de la
983 Société Géologique de France 180, 247–261. doi:10.2113/gssgfbull.180.3.247
984 Venkateswarlu, N.B., Raju, P.S.V.S.K., 1992. Fast isodata clustering algorithms. Pattern
985 Recognition 25, 335–342. doi:10.1016/0031-3203(92)90114-X
986 Verduzco, B., Fairhead, J.D., Green, C.M., MacKenzie, C., 2004. New insights into
987 magnetic derivatives for structural mapping. The Leading Edge 23, 116–119.
988 Vernhet, Y., Plaine, J., Trautmann, F., Pivette, B., avec la collaboration de Chevremont, P.,
989 Bourdillon, C., Cocherie, A., 2009 – Notice explicative, Carte géologique de France
990 (1/50 000), feuille Cossé-le-Vivien (355). Orléans : BRGM, 222 p. Carte géologique
991 par Vernhet, Y., Plaine, J., Trautmann, F., Clément J.P., 2009.
992 Vidal, P., 1980. L'évolution polyorogénique du Massif Armoricain : apport de la
993 géochronologie et de la géochimie isotopique du strontium. Mémoire de la Société
994 géologique Minérale de Bretagne, Rennes, 21,162-958
995 Vigneresse, J.-L., Brun, J.-P., 1983. Les leucogranites armoricains marqueurs de la
996 deformation regionale; apport de la gravimetrie. Bulletin de la Société Géologique de
997 France S7–XXV, 357–366. doi:10.2113/gssgfbull.S7-XXV.3.357
998 Vigneresse, J.-L., 1988. La fracturation post-hercynienne du Massif armoricain d'après les
999 données géophysiques. Géologie de la France 4, 3–10.
1000 Vigneresse, J.L., 1999. Intrusion level of granitic massifs along the Hercynian belt:
1001 balancing the eroded crust. Tectonophysics 307, 277–295. doi:10.1016/S0040-
1002 1951(99)00104-3
1003 Virlogeux, D., Roux, J. ets Guillemot, D., 1999. Apport de la géophysique à la connaissance
1004 géologique du Massif de Charroux-Civray et du socle Poitevin. Dans « Etude du Massif

1005 de Charroux-Civray ». Actes Journées Sciences CNRS-ANDRA, Poitiers, 13-14.
1006 10,33-61.
1007 Watts, M.S., and Williams, G.D., 1979. Faults rocks as indicators of progressive shear
1008 deformation in the Guingamp region, Brittany. Journal of Structural Geology, 1, 323-
1009 332.
1010 Weber, C., 1971. Le socle antépermien sous la bordure sud du bassin de Paris d'après les
1011 données géophysiques. Bulletin BRGM, section I n°3, 177–189.
1012 Weber, C., 1973. Le socle antétriasique sous la partie sud du Bassin de Paris d'après les
1013 données géophysiques. Bulletin BRGM, sect. II, n°3 et 4, 219-343.
1014 Wyns, R., Le Métour, J., 1983. Le Précambrien du massif vendéen. Etude détaillée de deux
1015 coupes de référence (coupes de l'Evre et de la Divatte) et synthèse des données
1016 récentes. Document BRGM, 68.
1017 Wyns, R., Lardeux, H., Moguedet, G., Duermael, G., Gruet, M., Biagi, R. avec la
1018 collaboration de Ballèvre, M., Chevremont, P., 1998. Notice explicative, carte
1019 géologique de la France (1/50 000), feuille Chemillé (483). BRGM, Orléans, 72 p.
1020
1021
1022

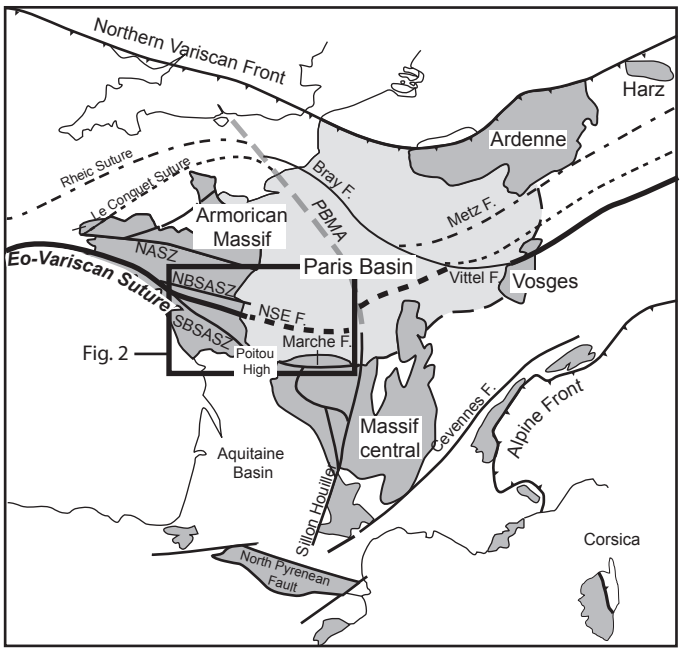

Fig. 1: Map of the Pre-Permian basement in France with Variscan sutures (modified from Faure, 2014). In dark grey: outcrops of the Variscan basement. NASZ: North Armorican Shear Zone, NBSASZ: Northern Branch of the South Armorican Shear Zone, SBSASZ: Southern Branch of the South Armorican Shear Zone, NSE F: Nort sur-Erdre Fault corresponding to the Eo-Variscan suture, PBMA: Paris Basin Magnetic Anomaly. In light grey: outcrop of the Meso-Cenozoic Paris Basin.

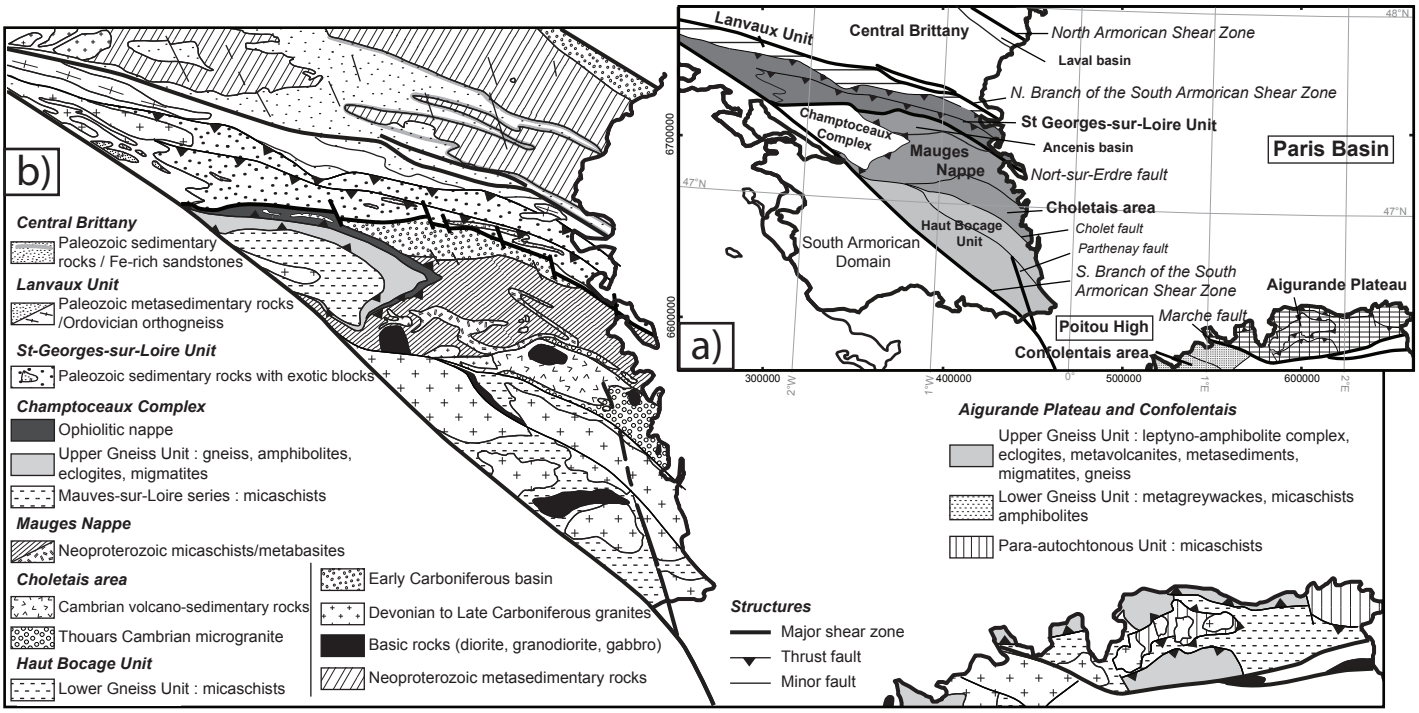

Fig. 2: Geological map of the southeastern part of the Armorican Massif and the northwestern part of the Massif Central: a) Major structures and litho-structural unit delimitations, b) Main lithologies within the litho-structural units (modified from Chantraine et al., 2003).

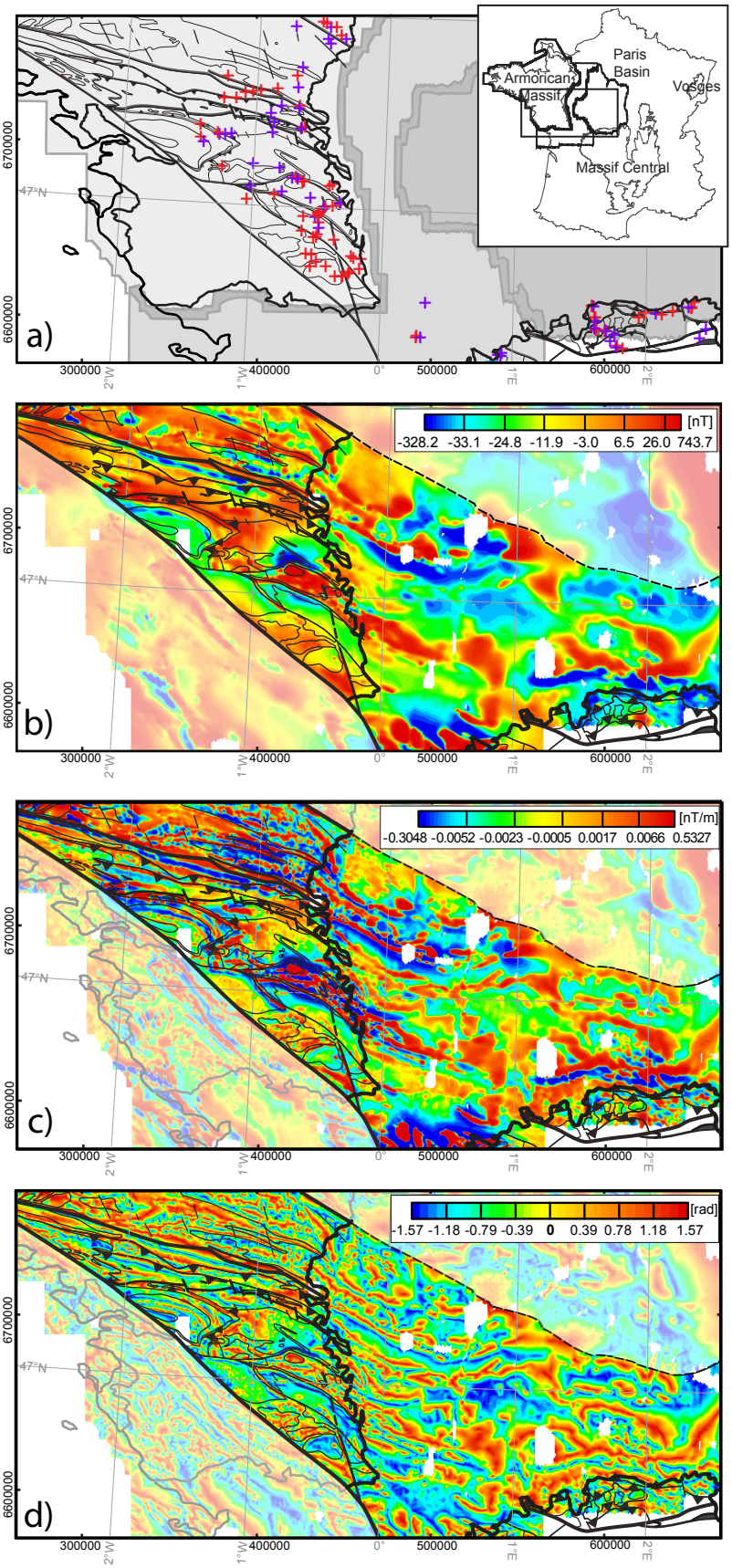

Fig. 3: **a)** Location map of the three aeromagnetic surveys used in this study. From west to east: Brittany, Pays de Loire (PaL), Région Centre. Crosses: location of the petrophysical field samples: in red: magnetic susceptibility only, in purple: magnetic susceptibility and density. **b)** Map of the magnetic anomaly reduced to the pole. **c)** Map of the magnetic vertical gradient. **d)** Map of the magnetic tilt derivative. Structural and lithological contours (thin black lines) and massif boundaries (thick black lines) are superimposed (modified from Chantraine et al., 2003).

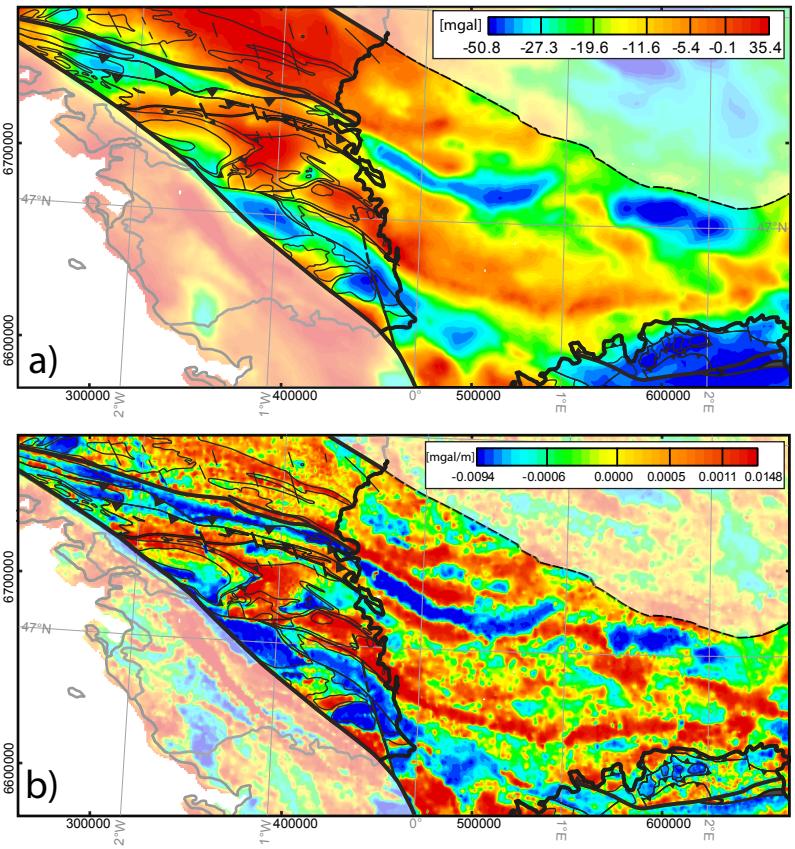

Fig. 4: **a)** Map of the Bouguer anomaly. **b)** Map of the vertical gradient of the Bouguer anomaly. Structural and lithological contours (thin black lines) and massif boundaries (thick black lines) are superimposed (modified from Chantraine et al., 2003).

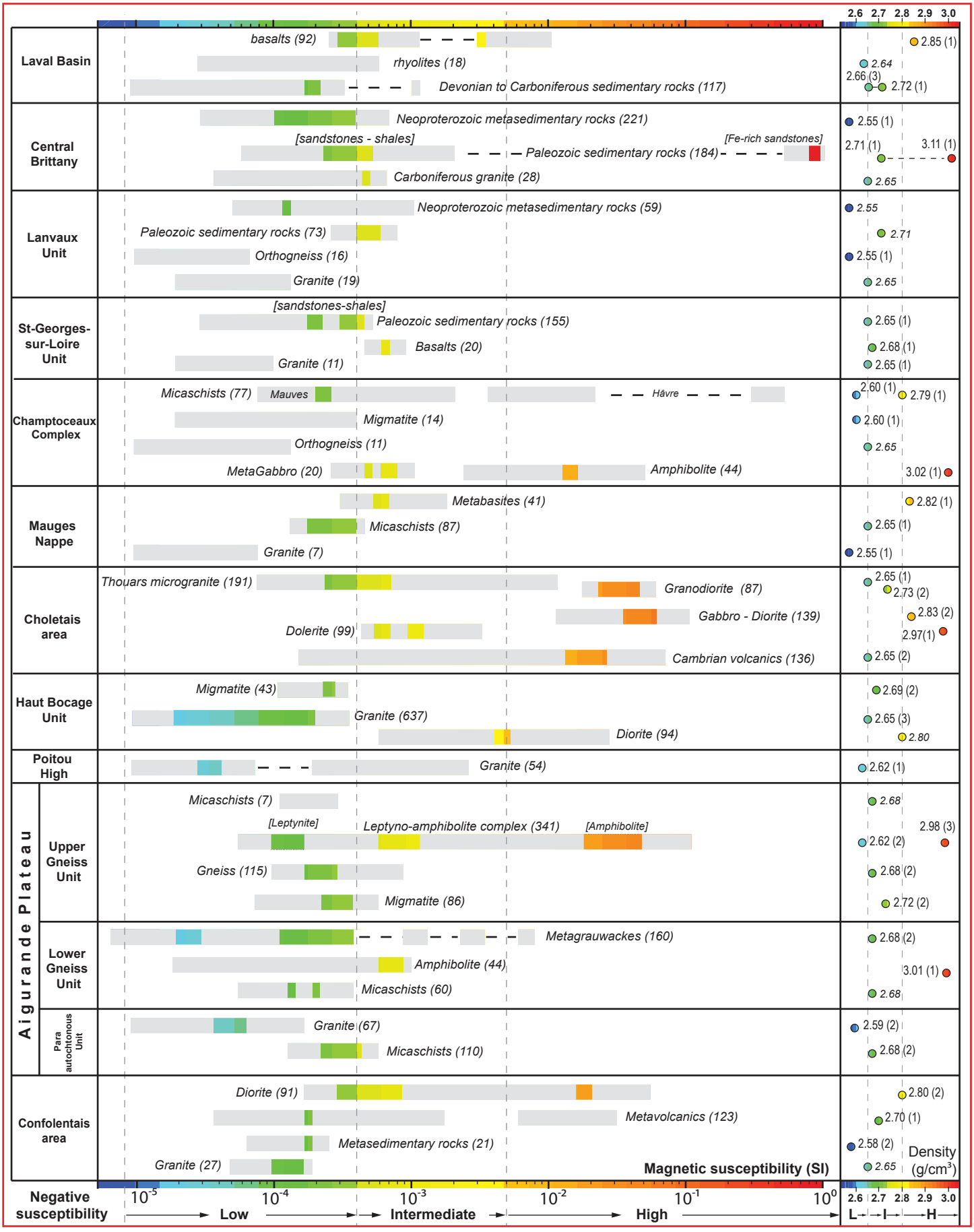

Fig. 5: Magnetic susceptibilities and average density values of the main lithologies sampled in the field, within each litho-structural unit. L: Low, I: Intermediate; H: High densities: refer to the text for explanations. In brackets: number of magnetic susceptibility measurements and number of density samples. Location of the sampling sites is documented in Fig. 3a.

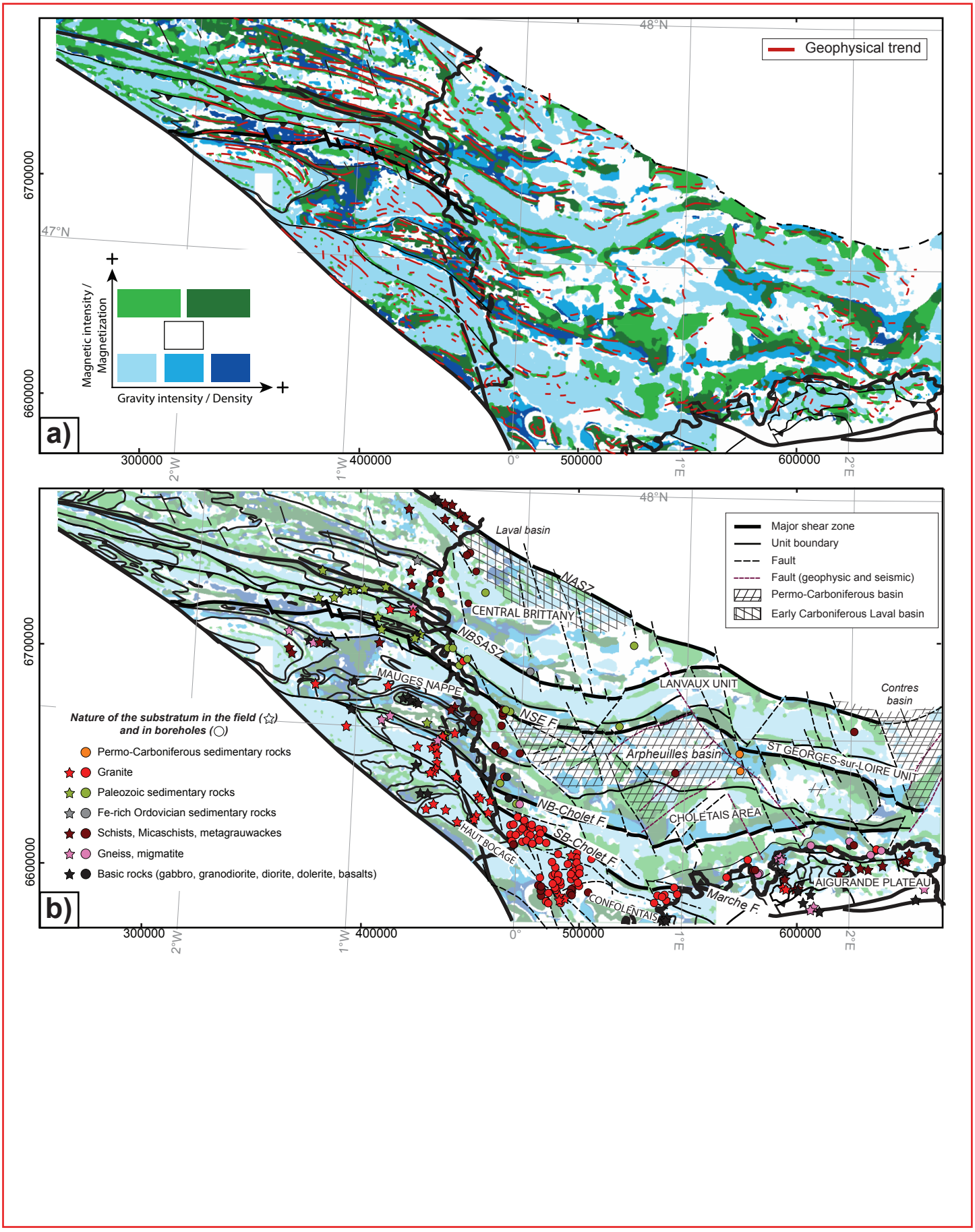

Fig. 6: a) Map of synthetized geophysical signatures resulting from the classification of the magnetic (magnetic anomaly reduced to the pole and magnetic tilt derivative) and gravity (vertical gradient of the Bouguer anomaly) signatures. Magnetic and gravity trends are superimposed (red lines).
b) Interpretative structural sketch map of the Pre-Mesozoic substratum, of the southwestern part of the Paris Basin, with the location of the Permo-Carboniferous basins, the lithology of the studied outcrops (colored stars) and the lithology of the substratum in boreholes (colored circles).

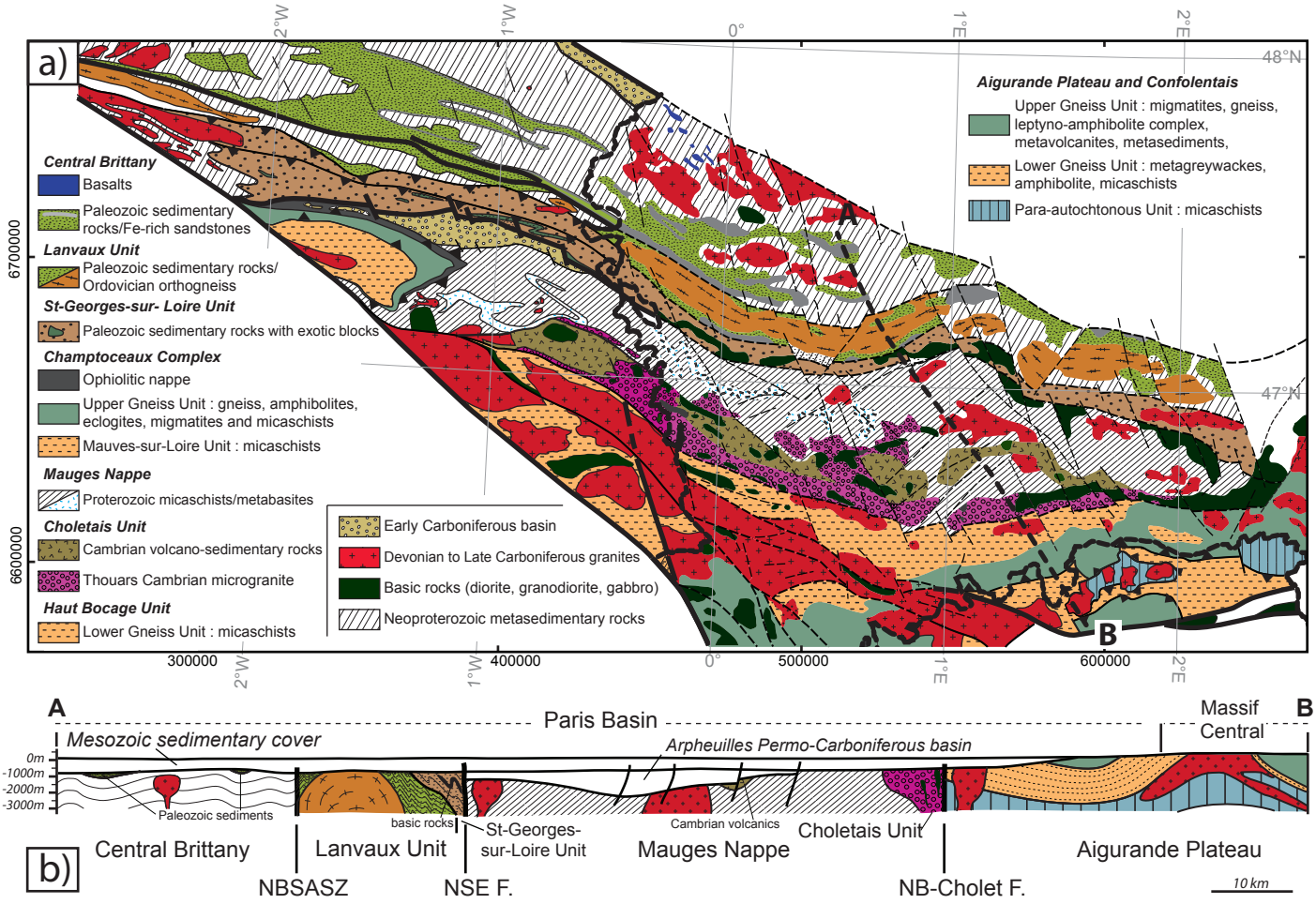

Fig. 7: **a)** Interpretative geological map of the Pre-Mesozoic substratum of the southwestern part of the Paris Basin. This map synthesizes the information coming from the potential field data (aeromagnetic and gravity enhanced maps), the classified geophysical signatures, the structural sketch map and the petrophysical characteristics of rock samples. For clarity reasons, Permo-Carboniferous basins are not represented in this map. The thick black dotted line locates the cross section presented in Fig.7b. **b)** Interpretative geological cross-section of the Pre-Mesozoic substratum of the southwestern part of the Paris Basin inferred from the geophysical information processed in this study, and the extension of the structures known in the field.

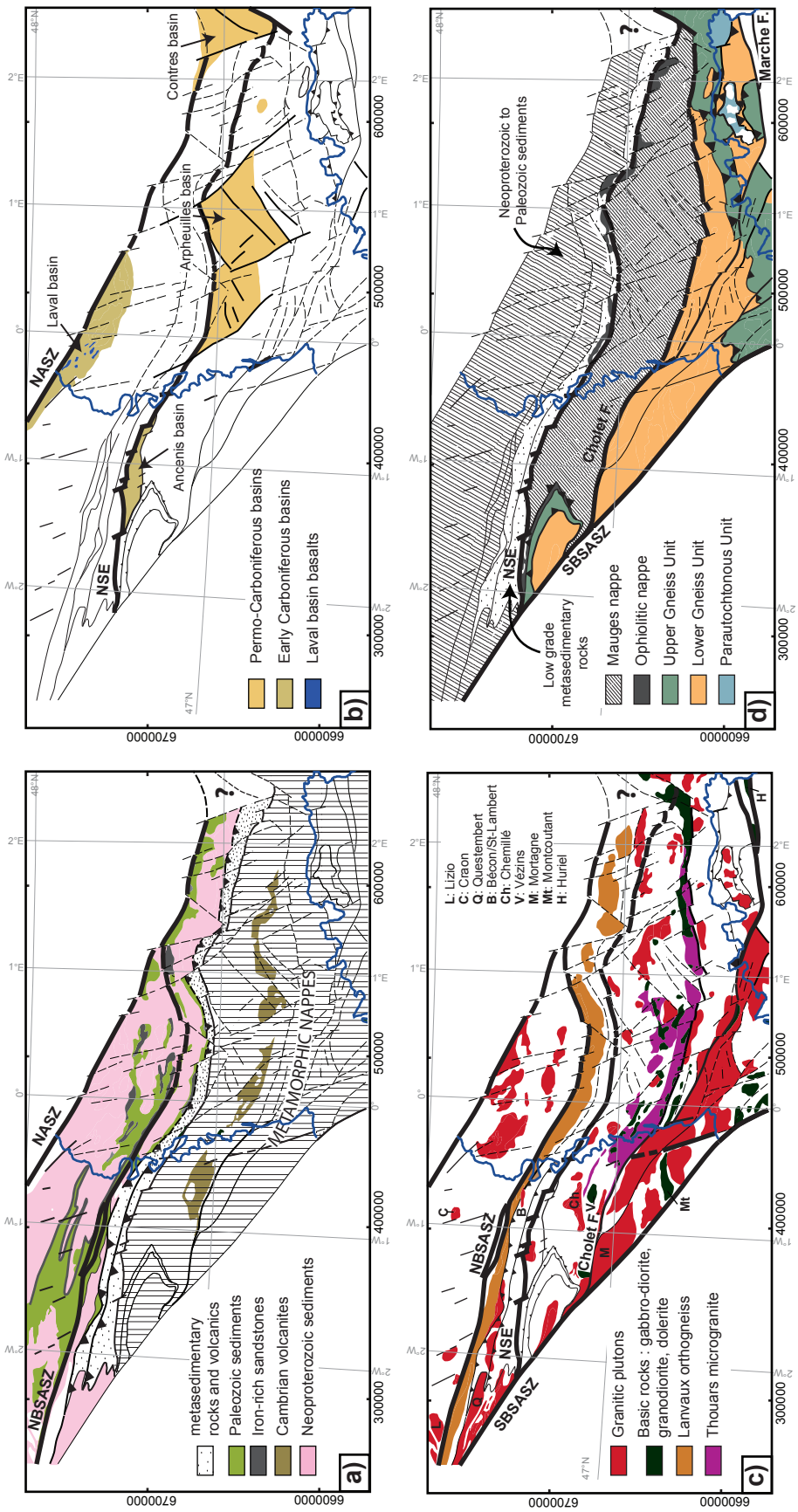

Fig. 8: Decomposition of the geological map into its main lithological ensemble: **a)** Sedimentary rocks and volcanites; **b)** Permo-Carboniferous basins, using geophysical and seismic data (modified from Beccaletto et al., 2015); **c)** magmatic intrusions; **d)** metamorphic nappes. Blue lines : massif boundaries (modified from Chantraine et *al*., 2003)